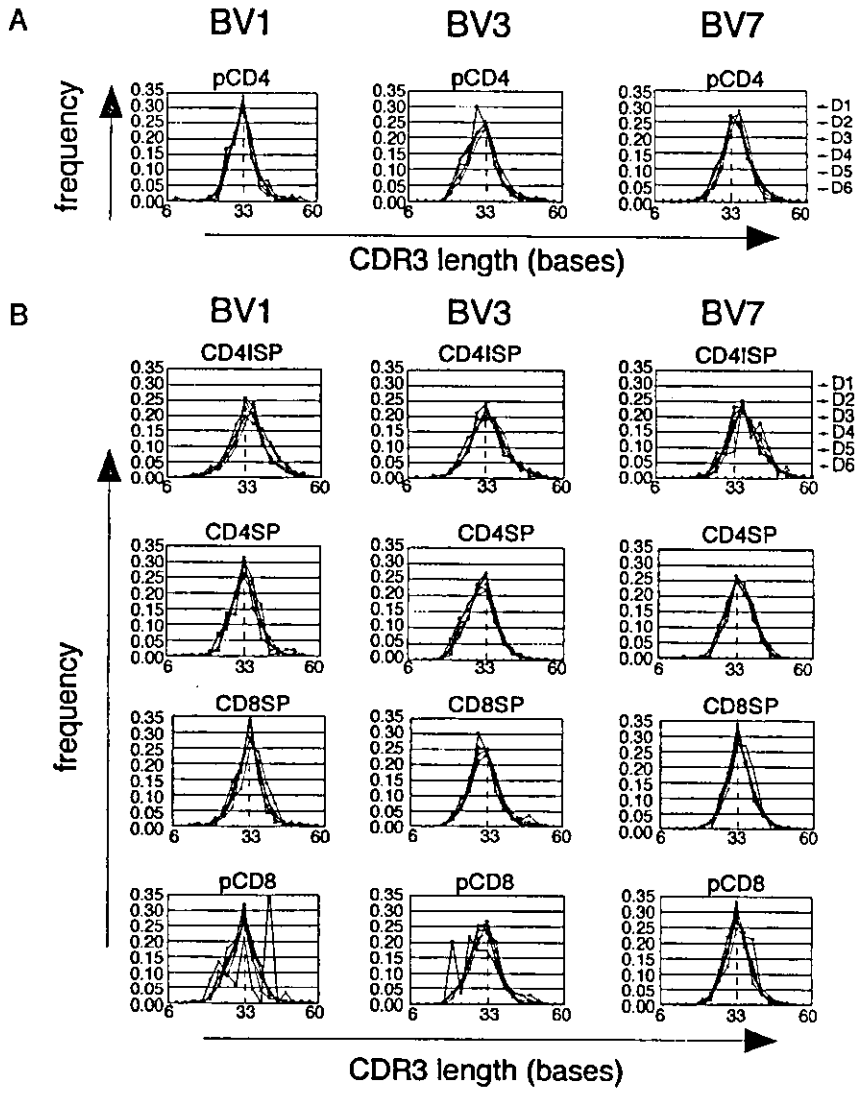

Fig. 2. TCRB CLS histograms of the BV1, 3 and 7 subsets of the peripheral lymphocytes and thymocytes. Distributions of the frequencies are presented in a line graph format. The data of the six donors (D1–D6) are shown as overlaid line graphs in each panel to illuminate BV-specific characteristics. (A) The histograms of the three BV subsets in their peripheral CD4 T cells. (B) The histograms of the CD4 ISP, CD4 SP and CD8 SP thymocytes, and peripheral CD8 T cells. Except for the CD4 ISP thymocytes, the histograms of each BV subset were similar. The BV1 and 3 subsets of the peripheral CD8 T cells from D4 were considerably biased, probably because of clonal expansions.

(Fig. 2B). In both SP populations, the CP frequencies of the BV1 subset were highest and those of the BV3 subset were lowest. The variances in the BV3 subset were largest. These differences were statistically significant (Fig. 3A and B).

Peripheral CD8 T cells from the same donors were analyzed in the same way. Their histograms were often biased since CD8 T cells are prone to large clonal expansions. Nevertheless, the BV-dependent characteristics were held well by the peripheral CD8 T cells (Figs 2B, and 3A and B).

In contrast, differences among the three subsets were not significant in the histograms of the CD4 ISP thymocytes (Fig. 2B). These histograms shared the same features, which were characterized by low CP and wide span regardless of BV gene use. In all of the three BV subsets, the CP frequencies and variances of the CD4 ISP thymocytes were different from those of the SP thymocytes and peripheral T cells in a statistically significant manner (Fig. 3A and B). The CP frequencies of CD4 ISP were significantly lower than those of CD4 SP in the BV1, 3, and 7 subsets ($P < 0.01$, $P < 0.05$ and $P < 0.05$ respectively), than those of CD8 SP ($P < 0.01$ for each subset), than those of peripheral CD4 ($P < 0.01$, $P < 0.05$ and $P < 0.01$ respectively) and than those of peripheral CD8 ($P < 0.01$, $P < 0.05$ and $P < 0.01$ respectively). The variances of CD4 ISP were significantly larger than those of CD4 SP in the

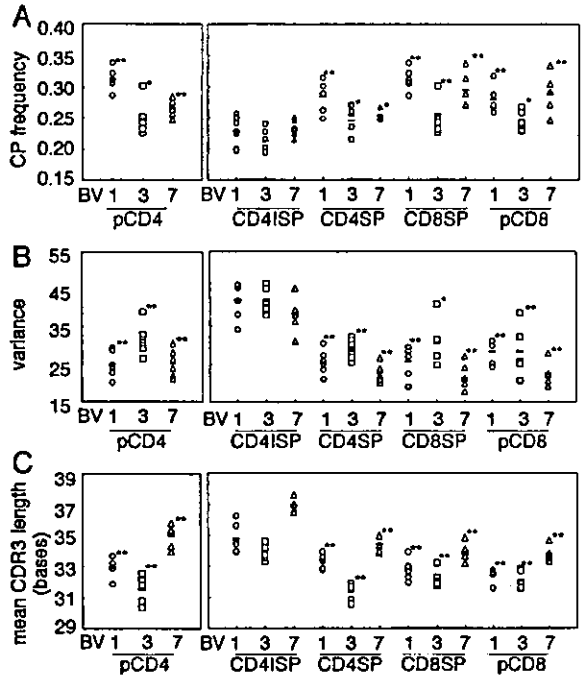

Fig. 3. Parameters to compare the TCR CLS histograms of CD4 ISP, CD4 SP and CD8 SP thymocytes, and peripheral CD4 and CD8 T cells. CP frequencies (A), variances (B) and mean CDR3 lengths (C) in the BV1, 3 and 7 subsets from the six donors are shown. Those of the peripheral CD8 T cells from D4 are excluded because of obvious biases. The Kruskal-Wallis test was used to compare the three parameters among the BV subsets. In the peripheral CD4, the three subsets were statistically different with respect to the CP frequency ($P < 0.005$), the variance ($P < 0.05$) and the mean CDR3 length ($P < 0.001$). In the CD4 ISP thymocytes, the three BV subsets were not significantly different with respect to the CP frequency and the variance, but significantly different with respect to the CDR3 length ($P < 0.002$). In the CD4 SP and CD8 SP thymocytes, the three BV subsets were different with respect to the CP frequency ($P < 0.05$ for both), the variances ($P < 0.02$ for both) and the mean CDR3 length ($P < 0.001$ and $P < 0.005$ respectively). The three BV subsets from peripheral CD8 were different with respect to the CP frequency ($P < 0.05$), the variance ($P < 0.05$) and the mean CDR3 length ($P < 0.005$). The Mann-Whitney test was used to compare the three parameters of the CD4 ISP thymocytes and the other populations. The CP frequencies of CD4 ISP were always lower than those of CD4 SP in the BV1, 3 and 7 subsets, than those of CD8 SP, than those of peripheral CD4, and than those of peripheral CD8. The variances of CD4 ISP were larger than those of CD4 SP in the BV1 3 and 7 subsets, than those of CD8 SP, than those of peripheral CD4, and than those of peripheral CD8. The mean CDR3 lengths of CD4 ISP were longer than those of CD4 SP, CD8 SP, peripheral CD4, and peripheral CD8 in all three subsets. $^{*}P < 0.05$ and $^{**}P < 0.01$ respectively in the Mann-Whitney test to compare each T cell population with the corresponding CD4 ISP population.

BV1, 3 and 7 subsets ($P < 0.01$ for each subset), than those of CD8 SP ($P < 0.01$, $P < 0.05$, and $P < 0.01$ respectively), than those of peripheral CD4 ($P < 0.01$ for each subset) and than those of peripheral CD8 ($P < 0.01$ for each subset).

As for the mean CDR3 length, the same differences among the three BV subsets were observed in the CD4 and CD8 SP thymocytes, and in the peripheral CD8 T cells (Fig. 3C). Unlike the distribution patterns, the differences in length were already seen in the CD4 ISP thymocytes (Fig. 3C). These results imply that positive and negative selections exert distinct effects on CLS distribution pattern and on CDR3 length.

Cluster analyses segregated the histograms of the CD4 and CD8 SP thymocytes into three groups, each of which contained primarily those of the same BV subset (Fig. 4C and D). The histograms of the peripheral CD8 T cells also fell into the three groups except for the histograms with biases (Fig. 4B). Notably, the same analysis of the histograms of the ISP thymocytes failed to discriminate BV gene use (Fig. 4E). This should be due to similarity of the distribution patterns and suggests that the difference in length alone is not enough for segregation.

BV- and co-receptor-dependent shortening of TCRB CDR3 length in the human thymus

It has been reported that TCR CDR3 shortens during transition from the ISP thymocytes to the SP thymocytes (21). This was observed in our studies of the mean CDR3 length; the CD4 ISP thymocytes had longer CDR3 than the other populations (Fig. 3C). To investigate this further, we analyzed plots of differences in frequency (ΔF) and skew values ($\Sigma\Delta F$), both of which have been defined by Yassai *et al.* (21,22). ΔF can be calculated by subtracting the CLS frequency of a given population from that of the other at the same length. A cluster of positive ΔF values on the right of an inflection point with a corresponding cluster of negative ΔF values on the other side indicates that the given population has shorter CDR3. $\Sigma\Delta F$ is the sum of ΔF values to the right of the inflection points. The ΔF plots and $\Sigma\Delta F$ were calculated by subtraction of the frequencies of the CD4 and CD8 SP thymocytes from those of the CD4 ISP thymocytes in the three BV subsets (Fig. 5A). Their patterns and positive $\Sigma\Delta F$ values showed that both SP thymocyte populations had shorter CDR3 than the CD4 ISP thymocytes irrespective of BV subset.

Interaction of TCR with endogenous antigens dictates CD4/CD8 lineage commitment during positive and negative selections in the thymus. This led us to assume that the shortening could be a function of the lineage if it is a consequence of TCR triggering. We then calculated ΔF between cells with different lineages; between the CD4 and CD8 SP thymocytes and between the peripheral CD4 and CD8 T cells (Fig. 5B). The ΔF plots and $\Sigma\Delta F$ showed that the TCR CDR3 length of CD4 lineage cells was shorter in the BV3 subset, whereas it was longer in the BV7 subset. No significant differences in CDR3 length were seen in the BV1 subset. Thus, differential shortening between CD4 and CD8 lineage cells was observed and it depended on BV gene use.

Additionally, the CD4 SP thymocytes and the peripheral CD4 T lymphocytes, as well as the CD8 SP thymocytes and the peripheral CD8 T lymphocytes, were compared. The results showed that CDR3 of CD4 or CD8 lineage cells do not shorten in the peripheral blood (data not shown).

Discussion

The present study has elucidated how TCR CDR3 length repertoires of CD4 and CD8 T cells in different BV subsets develop in the human thymus and peripheral blood. The CDR3 length repertoires had BV-dependent distribution patterns.

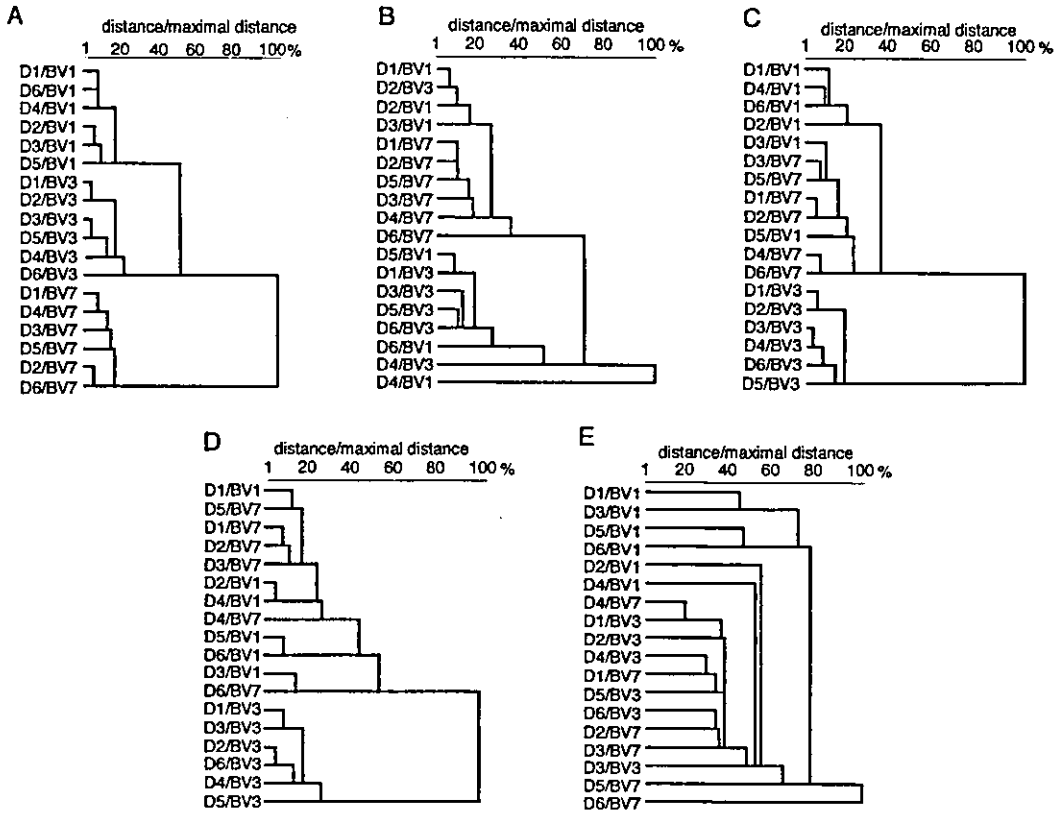

Fig. 4. Cluster analyses of the histograms of individual T cell populations from the six donors. Based on 18 histograms of peripheral CD4 (A) and CD8 (B) T cells, CD4 SP (C) and CD8 SP (D) thymocytes, and CD4 ISP thymocytes (E), the distance of every combination of two histograms was calculated with Ward's method and the Euclidean distance. All calculated distances divided by the maximal distance are shown in a dendrogram. Listed on the left are the BV subsets and the identification of donors that the individual histograms originated from. The BV1 and 3 subsets of the peripheral CD8 T cells from D4 had biased CLS histograms.

They were shaped during thymic selections and maintained in the peripheral blood. In contrast, the BV-dependent differences in the TCR CDR3 length were observed throughout lymphocyte development. The CDR3 became shorter during thymic selections, but did not change the BV-dependent differences seen before the selections. Finally, the degrees of the shortening differed between CD4 and CD8 lineage cells, and also were dependent on BV gene use. The repertoires of peripheral lymphocytes reflected directly those of mature SP thymocytes except for biases induced by clonal expansions.

Although it was known that different CDR3 lengths were preferred by different BV subsets, the BV-dependent distribution patterns are disclosed here for the first time. Unlike the difference in length, the different patterns become evident during positive and negative selections, accompanied by an increase of the CP frequency and narrowing of the distribution span. This argues that they are shaped under the pressure of positive and negative selections in the thymus. Most studies that employed the TCR CLS technique disregarded the differences, probably because the technique was used for identification of gross changes.

We have found that the distribution patterns of three gene members of the BV7 family shared the same characteristics. This ensures that the CLS histograms generated with the primer specific to BV7 family genes were not artifacts. In this regard, we have found that different gene members of the BV6 family could have similar distribution patterns (Fig. 1B). Also, both BV3 and 11 subsets shared histograms with low CP frequencies and large variances. Arden *et al.* (29) pointed out that these two genes are closely related both structurally and in their CDR3 sequences. According to their TCRBV gene classification, BV1, 3 and 7 fall into different groups. These facts argue that the BV-dependent differences could be attributable to the structure of TCRβ chains.

Using murine thymus, Pannetier *et al.* (23) observed that different BV subsets prefer different TCR CDR3 lengths. We found that the BV-dependent difference in mean TCR length already occurred in the CD4 ISP thymocytes. This implies that the difference is regulated by TCR rearrangement. Also, since the CD4 ISP thymocytes with complete TCRB gene rearrangement are under pressure of subsequent β selection for association with pre-Tα chains, the β selection could contribute to the difference formation. Moreover, the CLS histograms

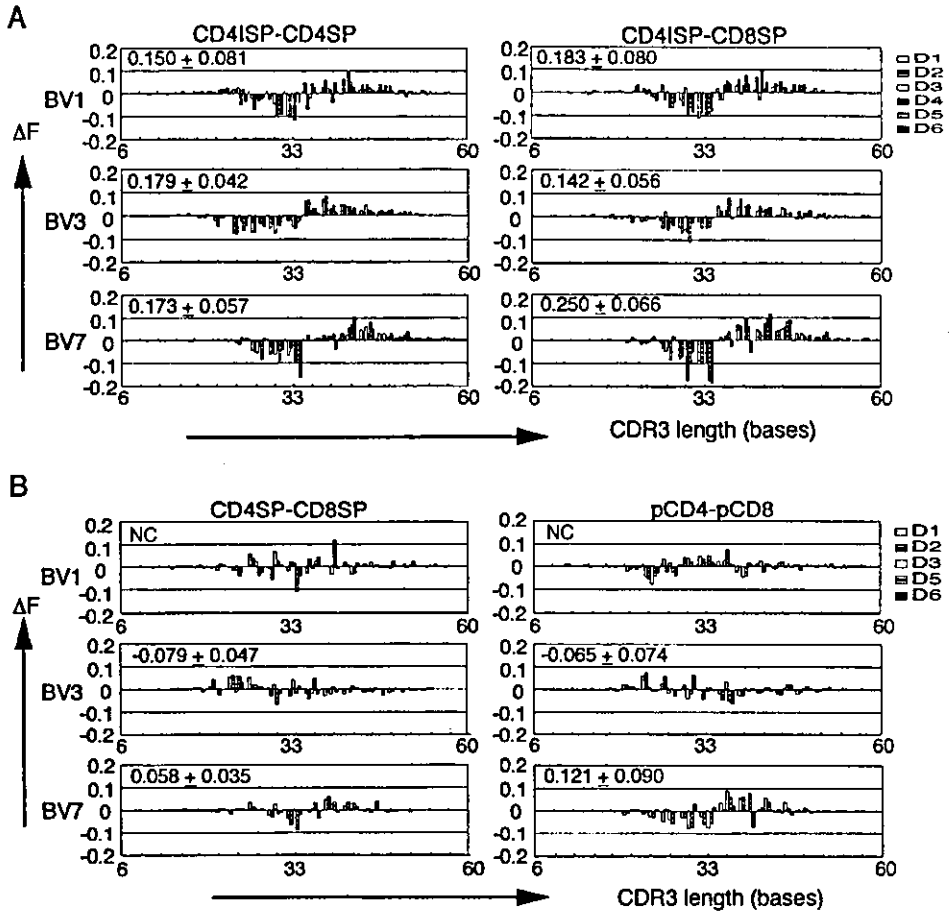

Fig. 5. Comparison of TCR CDR3 length in different CD4/CD8 lineage cells. Plotted are ΔF that were calculated by subtracting the frequencies in the CD4 and CD8 SP thymocytes from those in the ISP thymocytes (A: CD4 ISP – CD4 SP and CD4 ISP – CD8 SP respectively), and by subtracting the frequencies in the CD8 SP thymocytes from those in the CD4 SP thymocytes and those in the peripheral CD8 T cells from those in the peripheral CD4 T cells (B: CD4 SP – CD8 SP and peripheral CD4 – peripheral CD8 respectively). In order to quantify the shortening, the means ± SD of $\Sigma\Delta F$ derived from the six donors were calculated (shown in the panels). In (B), where the data from D4 have been excluded, $\Sigma\Delta F$ values of the BV3 subsets were all negative in both subtractions, while $\Sigma\Delta F$ values of the BV7 subsets were all positive. $\Sigma\Delta F$ values were not calculated for the BV1 subset because no inflection points were found in the ΔF plots. NC, not calculated.

of the BV1, 3 and 7 subsets of the CD4 ISP thymocytes were similar, but not necessarily identical (Fig. 2B), suggesting that the rearrangement and/or β selection may have a subsidiary effect in shaping the CLS distribution patterns.

To address further if the rearrangement *per se* regulates the BV-dependent difference in CDR3 length, we tried to amplify non-productively recombined TCRBV1, 3 and 7 genes from peripheral T lymphocytes that do not express TCRVβ1, 3 or 7. However, even from $>10^7$, a sufficient amount of the rearranged genes could not be amplified for the TCR CLS analyses. This was consistent with the fact that the TCRB CLS patterns of the CD4 ISP thymocytes always had 3-base pair spacing, indicating that all transcripts were in-frame. The 3-base spacing was also observed by Yassai *et al.* (21) who examined TCRB genomic DNA derived from the same population. It is known that 85% of CD4 ISP thymocytes retain the TCRB germline configuration, while only 5% express rearranged TCRB gene products (9). Thus, thymocytes with out-of-frame TCRB rearrangements must be diluted out quickly by those expressing complete TCRβ/pre-Tα and become undetectable with conventional technologies.

In separate experiments, we have assessed the mean TCR CDR3 lengths of the other BV subsets and found that the BV subsets with similar CLS patterns do not necessarily have similar CDR3 length (data not shown). The differences in shortening between CD4 and CD8 lineage cells were not a function of the distribution patterns (data not shown). Thus, distribution pattern and length appeared to be regulated independently.

Yassai *et al.* (21,22) reported TCR shortening in the human and murine thymi. By examining murine thymocytes for the BV1–BJ2 recombinants, they have shown that the shortening

occurs to a larger extent in the CD4 lineage cells than in the CD8 lineage cells. They failed to see differential shortening in humans and suggested a distinct regulation for human thymocytes. However, we observed a clear difference between the CD4 and CD8 T cells. We found that the differential shortening was a function of BV gene use. These data imply that the shortening in humans is regulated by antigen recognition by TCR.

The TCR shortening could be affected by allelic variations of MHC gene products, and differential shortening between CD4 and CD8 lineage cells could be due to differential orthogonal geometry of TCR and antigenic peptide in the grooves of MHC class I and II molecules (22). However, the differences in mean CDR3 length were preserved throughout the thymic selections. The CD4 and CD8 lineage cells share the same CLS distribution patterns. Thus, although limitations in sample collection did not allow us to investigate the effects of HLA variations, the geometry should not be the only factor regulating CDR3 length repertoire.

Development of the TCRB CDR3 length repertoire is regulated delicately in the thymus. Peripheral selections have little effect unless T cell clones expand massively in response to immunological insults. Elucidation of these thymic regulations may shed more light on molecular interaction of TCR with self-peptide–MHC in the thymus.

Acknowledgements

This study was supported by a grant from the Ministry of Health, Labor and Welfare, Japan. The authors thank Dr Takeshi Hiramatsu at Tokyo Women's Medical University for providing us with thymus and peripheral blood samples.

Abbreviations

ΔF	differences in frequency
$\Sigma\Delta F$	skew value
CDR	complementarity-determining region
CLS	CDR3 length spectratyping
CP	central peak
ISP	immature single positive
SP	single positive

References

1 Garboczi, D. N., Ghosh, P., Utz, U., Fan, Q. R., Biddison, W. E. and Wiley, D. C. 1996. Structure of the complex between human T-cell receptor, viral peptide and HLA-A2. *Nature* 384:134.
2 Garcia, K. C., Degano, M., Stanfield, R. L., Brunmark, A., Jackson, M. R., Peterson, P. A., Teyton, L. and Wilson, I. A. 1996. An αβ T cell receptor structure at 2.5 Å and its orientation in the TCR-MHC complex. *Science* 274:209.
3 Jorgensen, J. L., Reay, P. A., Ehrich, E. W. and Davis, M. M. 1992. Molecular components of T-cell recognition. *Annu. Rev. Immunol.* 10:835.
4 Wilson, R. K., Lai, E., Concannon, P., Barth, R. K. and Hood, L. E. 1988. Structure, organization and polymorphism of murine and human T-cell receptor α and β chain gene families. *Immunol. Rev.* 101:149.
5 Davis, M. M. 1990. T cell receptor gene diversity and selection. *Annu. Rev. Biochem.* 59:475.
6 Rammensee, H. G. 1995. Chemistry of peptides associated with MHC class I and class II molecules. *Curr. Opin. Immunol.* 7:85.
7 Matsushita, S., Takahashi, K., Motoki, M., Komoriya, K., Ikagawa, S. and Nishimura, Y. 1994. Allele specificity of structural requirement for peptides bound to HLA-DRB1*0405 and -DRB1*0406 complexes: implication for the HLA-associated susceptibility to methimazole-induced insulin autoimmune syndrome. *J. Exp. Med.* 180:873.
8 Ramiro, A. R., Trigueros, C., Marquez, C., San Millan, J. L. and Toribio, M. L. 1996. Regulation of pre-T cell receptor (pTα-TCRβ) gene expression during human thymic development. *J. Exp. Med.* 184:519.
9 Blom, B., Verschuren, M. C., Heemskerk, M. H., Bakker, A. Q., van Gastel-Mol, E. J., Wolvers-Tettero, I. L. M., van Dongen, J. J. M. and Spits, H. 1999. TCR gene rearrangements and expression of the pre-T cell receptor complex during human T-cell differentiation. *Blood* 93:3033.
10 Fehling, H. J., Krotkova, A., Saint-Ruf, C. and von Boehmer, H. 1995. Crucial role of the pre-T-cell receptor α gene in development of αβ but not γδ T cells. *Nature* 375:795.
11 Sebzda, E., Mariathasan, S., Ohteki, T., Jones, R., Bachmann, M. F. and Ohashi, P. S. 1999. Selection of the T cell repertoire. *Annu. Rev. Immunol.* 17:829.
12 Pannetier, C., Even, J. and Kourilsky, P. 1995. T-cell repertoire diversity and clonal expansions in normal and clinical samples. *Immunol. Today* 16:176.
13 Hingorani, R., Choi, I. H., Akolkar, P., Gulwani, A. B., Pergolizzi, R., Silver, J. and Gregersen, P. K. 1993. Clonal predominance of T cell receptors within the CD8+ CD45RO+ subset in normal human subjects. *J. Immunol.* 151:5762.
14 Gorski, J., Yassai, M., Zhu, X., Kissela, B., Keever, C. and Flomenberg, N. 1994. Circulating T cell repertoire complexity in normal individuals and bone marrow recipients analyzed by CDR3 size spectratyping. Correlation with immune status. *J. Immunol.* 152:5109.
15 Schwab, R., Szabo, P., Manavalan, J. S., Weksler, M. E., Posnett, D. N., Pannetier, C., Kourilsky, P. and Even, J. 1997. Expanded CD4+ and CD8+ T cell clones in elderly humans. *J. Immunol.* 158:4493.
16 Maccalli, C., Farina, C., Sensi, M., Parmiani, G. and Anichini, A. 1997. TCR β-chain variable region-driven selection and massive expansion of HLA-class I-restricted antitumor CTL lines from HLA-A*0201+ melanoma patients. *J. Immunol.* 158:5902.
17 Lin, M. Y. and Welsh, R. M. 1998. Stability and diversity of T cell receptor repertoire usage during lymphocytic choriomeningitis virus infection of mice. *J. Exp. Med.* 188:1993.
18 Sourdive, D. J., Murali, K. K., Altman, J. D., Zajac, A. J., Whitmire, J. K., Pannetier, C., Kourilsky, P., Evavold, B., Sette, A. and Ahmed, R. 1998. Conserved T cell receptor repertoire in primary and memory CD8 T cell responses to an acute viral infection. *J. Exp. Med.* 188:71.
19 Nishio, J., Suzuki, M., Miyasaka, N. and Kohsaka, H. 2001. Clonal biases of peripheral CD8 T cell repertoire directly reflect local inflammation in polymyositis. *J. Immunol.* 167:4051.
20 Moss, P. A. and Bell, J. I. 1995. Sequence analysis of the human αβ T-cell receptor CDR3 region. *Immunogenetics* 42:10.
21 Yassai, M. and Gorski, J. 2000. Thymocyte maturation: selection for in-frame TCR α-chain rearrangement is followed by selection for shorter TCR β-chain complementarity-determining region 3. *J. Immunol.* 165:3706.
22 Yassai, M., Ammon, K., Goverman, J., Marrack, P., Naumov, Y. and Gorski, J. 2002. A molecular marker for thymocyte-positive selection: selection of CD4 single-positive thymocytes with shorter TCRB CDR3 during T cell development. *J. Immunol.* 168:3801.
23 Pannetier, C., Cochet, M., Darche, S., Casrouge, A., Zoller, M. and Kourilsky, P. 1993. The sizes of the CDR3 hypervariable regions of the murine T-cell receptor β chains vary as a function of the recombined germ-line segments. *Proc. Natl Acad. Sci. USA* 90:4319.
24 Hall, M. A. and Lanchbury, J. S. 1995. Healthy human T-cell receptor β-chain repertoire. Quantitative analysis and evidence for J β-related effects on CDR3 structure and diversity. *Hum. Immunol.* 43:207.
25 Nanki, T., Kohsaka, H. and Miyasaka, N. 1998. Development of human peripheral TCRBJ gene repertoire. *J. Immunol.* 161:228.
26 Kohsaka, H., Taniguchi, A., Chen, P. P., Ollier, W. E. R. and

Carson, D. A. 1993. The expressed T cell receptor V gene repertoire of rheumatoid arthritis monozygotic twins:rapid analysis by anchored polymerase chain reaction and enzyme-linked immunosorbent assay. *Eur. J. Immunol.* 23:1895.
27 Callahan, J. E., Kappler, J. W. and Marrack, P. 1993. Unexpected expansions of CD8-bearing cells in old mice. *J. Immunol.* 151:6657.
28 Novak, E. J., Liu, A. W., Nepom, G. T. and Kwok, W. W. 1999. MHC class II tetramers identify peptide-specific human CD4+ T cells proliferating in response to influenza A antigen. *J. Clin. Invest.* 104:R63.
29 Arden, B., Clark, S. P., Kabelitz, D. and Mak, T. W. 1995. Human T-cell receptor variable gene segment families. *Immunogenetics* 42:455.
30 Williams, A. F., Strominger, J. L., Bell, J., Mak, T. W., Kappler, J., Marrack, P., Arden, B., Lefranc, M. P., Hood, L., Tonegawa, S. and Davis, M. 1993. Nomenclature for T-cell receptor (TCR) gene segments of the immune system. *WHO Bull.* 71:113.

GITR Activation Induces an Opposite Effect on Alloreactive CD4$^+$ and CD8$^+$ T Cells in Graft-Versus-Host Disease

Stephanie J. Muriglan,[1] Teresa Ramirez-Montagut,[1] Onder Alpdogan,[1] Thomas W. van Huystee,[1] Jeffrey M. Eng,[1] Vanessa M. Hubbard,[1] Adam A. Kochman,[1] Kartono H. Tjoe,[1] Carlo Riccardi,[3] Pier Paolo Pandolfi,[2] Shimon Sakaguchi,[4,5] Alan N. Houghton,[1] and Marcel R.M. van den Brink[1]

[1]*Department of Medicine and Immunology and* [2]*Department of Pathology, Memorial Sloan-Kettering Cancer, New York, NY 10021*

[3]*Department of Clinical and Experimental Medicine, Perugia University Medical School, 06100 Perugia, Italy*

[4]*Department of Experimental Pathology, Institute for Frontier Medical Sciences, Kyoto University, Kyoto 606-8507, Japan*

[5]*Laboratory for Immunopathology, Institute of Physical and Chemical Research, Research Center for Allergy and Immunology, Yokohama 230-0045, Japan*

Abstract

Glucocorticoid-induced tumor necrosis factor receptor family-related gene (GITR) is a member of the tumor necrosis factor receptor (TNFR) family that is expressed at low levels on unstimulated T cells, B cells, and macrophages. Upon activation, CD4$^+$ and CD8$^+$ T cells up-regulate GITR expression, whereas immunoregulatory T cells constitutively express high levels of GITR. Here, we show that GITR may regulate alloreactive responses during graft-versus-host disease (GVHD) after allogeneic bone marrow transplantation (BMT). Using a BMT model with major histocompatibility complex class I and class II disparity, we demonstrate that GITR stimulation in vitro and in vivo enhances alloreactive CD8$^+$CD25$^-$ T cell proliferation, whereas it decreases alloreactive CD4$^+$CD25$^-$ proliferation. Allo-stimulated CD4$^+$CD25$^-$ cells show increased apoptosis upon GITR stimulation that is dependent on the Fas–FasL pathway. Recipients of an allograft containing CD8$^+$CD25$^-$ donor T cells had increased GVHD morbidity and mortality in the presence of GITR-activating antibody (Ab). Conversely, recipients of an allograft with CD4$^+$CD25$^-$ T cells showed a significant decrease in GVHD when treated with a GITR-activating Ab. Our findings indicate that GITR has opposite effects on the regulation of alloreactive CD4$^+$ and CD8$^+$ T cells.

Key words: transplantation immunology • in vivo animal models • immune regulation • lymphocyte activation • T lymphocyte subsets

Introduction

Glucocorticoid-induced tumor necrosis factor receptor family-related gene (GITR), also known as TNFRSF18, is a type I transmembrane protein with high homology to other members of the TNFR family, including 4-1BB, CD27, and OX40 (1, 2). As with other members of the TNFR family, signaling through GITR may induce cell survival or cell death. Stimulation of human and mouse T cells through GITR induces NFκB activation via the TRAF2–NIK signaling pathway (3, 4). The intracellular domain of GITR binds Siva, a cytoplasmic molecule that contains a death domain, and may signal for induction of

S.J. Muriglan and T. Ramirez-Montagut contributed equally to this work.
The online version of this article contains supplemental material.

Address correspondence to Teresa Ramirez-Montagut, Memorial Sloan-Kettering Cancer Center, Kettering 425, Mailbox 111, 1275 York Ave., New York, NY 10021. Phone: (212) 639-5607; Fax: (917) 432-2375; email: ramirezt@mskcc.org

This work was presented at the American Society of Hematology Annual Meeting in 2003, the American Society for Blood and Marrow Transplantation in 2004, the American Association for Cancer Research Annual Meeting in 2004, and the American Association for Immunologists in 2004 in abstract form.

Abbreviations used in this paper: AICD, activation-induced cell death; BMT, BM transplantation; CFSE, carboxyfluorescein succinimidyl ester; GITR, glucocorticoid-induced tumor necrosis factor receptor family-related gene; GITRL, GITR ligand; sGITR, soluble GITR; TCD, T cell–deleted.

cell death (5). Four splice variants that differ in GITR intracellular domain have been identified. These cytoplasmic distinctions may generate different signaling events, and one of them may encode a decoy receptor (6). Mouse macrophages express constitutive levels of GITR–GITR ligand (GITRL) and stimulation with soluble GITR (sGITR) leads to an increased production of nitric oxide (7), COX-2 (8), and MMP-9 (9). Macrophage stimulation with sGITR signals through the Rel–NFκB pathway, but it remains to be determined if sGITR is an agonist or antagonist of GITR signaling (10). In vitro studies using murine GITRL protein and GITRL transfectants demonstrate that GITR signaling can enhance or inhibit the proliferation of Ag-stimulated T helper 1, T helper 2, and naive $CD4^+$ T cells from TCR transgenic mice depending on the concentration of the cognate peptide, thus suggesting that GITR can function as a costimulatory receptor for TCR activation (11). Mice deficient for GITR have normal lymphoid and T cell development (12). However, experiments with $GITR^{-/-}$ T cells showed hyperproliferation to TCR stimulation, increased IL-2 production, increased IL-2 receptor α chain (CD25) expression, and increased susceptibility to activation-induced cell death (AICD) (12). The human GITRL has been detected in several tissues including ovary, testis, kidney, pancreas, PBLs, lymph nodes, and human umbilical vein endothelial cells (3, 4). Mouse GITRL expression has been demonstrated in macrophages, B cells, and both immature and mature dendritic cells (11, 13, 14). Stimulation with mitogens or LPS results in a temporary increase in the expression levels of GITRL, which is regulated by the transcription factor NF-1(11).

Mouse models for autoimmune disease suggest that GITR activation may break self-tolerance and induce autoimmunity presumably by inhibition of immunoregulatory T cell suppression (15, 16). In vivo administration of the agonist anti-GITR Ab, DTA-1, does not deplete GITR-expressing cells (15), but the mechanism by which immunoregulatory T cells are inhibited by GITR activation or the effect of GITR stimulation on other cell types such as B cells has not been defined. Apart from in vitro studies suggesting a costimulatory role for GITR in $CD4^+$ T cell activation (11, 15, 17, 18), the function of GITR on $CD4^+CD25^-$ and especially $CD8^+CD25^-$ remains largely unknown. Because GITR expression is up-regulated upon stimulation of T cells, we were interested in studying GITR expression and activation of alloreactive $CD4^+$ $CD25^-$ and $CD8^+CD25^-$ T cells and its effects on the development of GVHD.

Materials and Methods

Reagents and Antibodies. The DTA-1 hybridoma was generated as described previously (15), and rat IgG control Ab was obtained from Anogen. Antimurine CD16/CD32 FcR block (2.4G2), TNFR1 (55R-593), TNF (MP6-XT3), and all of the following fluorochrome labeled and purified antibodies against murine Ag were obtained from BD Biosciences: CD4 (RM4-5), CD8 (53-6.7), CD62L (MEL-14), CD122 (TM-B1), CD44 (IM7), CD45R/B220 (RA3-6B2), Gr-1 (RB6-8C5), CD25 (PC61), CD69 (H1.2F3), H-2Kb (AF6-88.5), Ly 9.1 (30C7), Fas (JO2), FasL (MFL3), isotype controls; rat IgG2a-κ (R35-95), rat IgG2a-λ (B39-4), rat IgG2b (A95-1), hamster IgG group 1 liter (Ha4/8), streptavidin-FITC, -PE, and -PCP. Biotinylated anti-murine GITR (BAF524) was obtained from R&D Systems. Carboxyfluorescein succinimidyl ester (CFSE) was obtained from Molecular Probes.

In Vitro Assays. Tissue culture medium consisted of RPMI 1640 or DMEM supplemented with 10% heat inactivated FBS, 100 U/ml penicillin, 100 μg/ml streptomycin, 2 mM L-glutamine, and 50 μM of 2-mercaptoethanol (2-ME). For Ab stimulation, 1 μg/ml anti-CD3 and anti-CD28 was used. For proliferation assays, 10 μg/ml DTA-1 or rat IgG control Ab was used. T cells were purified, and 10^5 cells/well were incubated for 6 d with irradiated (2,000 cGy) splenocytes as stimulators (2×10^5 cells/well) in 96-well plates. Cultures were pulsed during the final 18 h with 1 μCi/well thymidine and harvested with Topcount Harvester (19). Cell proliferation was determined as counts per minute.

BMT and T Cell Purification. Female C57BL/6 ($H\text{-}2^b$), BALB/c ($H\text{-}2^k$), B10.BR ($H\text{-}2^k$), CBA/J($H\text{-}2^k$), *lpr* (B6.MRL-Fas^{lpr}), and C57BL/6 ($Ly5.1^+$) were obtained from The Jackson Laboratory. $GITR^{-/-}$ mice (C57BL/6 × 129/SvJ) were generated at Memorial Sloan-Kettering (12). All mice were used between 8–10 wk of age. BM cells were removed aseptically from femurs and tibias and depleted of T cells by incubation with anti-Thy-1.2 for 30 min at 4°C followed by incubation with Low-TOX-M rabbit complement (Cedarlane Laboratories) for 40 min at 37°C. Cells (5×10^6 BM cells without splenic T cells) were resuspended in DMEM (Life Technologies) and transplanted by tail vein infusion (0.25 ml total volume) into lethally irradiated recipients on day 0. On day 0, before transplantation, recipients received 900 cGy (BALB/c) or 1300 cGy (CBA/J) total body irradiation (^{137}Cs source) as a split dose with a 3-h interval between doses (to reduce gastrointestinal toxicity). T cells were obtained from spleens, purified over a nylon wool column, or positively selected with anti-CD5 magnetic beads. $CD4^+CD25^-$ and $CD8^+CD25^-$ T cells were purified with magnetic beads (~90% purity; Miltenyi Biotec) or sorted with Moflow (~98–99% purity; DakoCytomation). Experiments were performed with sorted fractions and confirmed with bead-purified T cells. In brief, $CD25^-$ T cells were obtained by negative selection of splenocytes treated with anti-CD25 PE-conjugated Ab and anti-PE microbeads. $CD4^+$ and $CD8^+$ fractions were separated by positive selection for anti-CD4 or anti-CD8 antibodies conjugated to microbeads. Mice were housed in sterilized micro-isolator cages and received normal chow and autoclaved hyperchlorinated drinking water (pH 3.0). All experiments were performed in accordance with our institutional guidelines.

Assessment of GVHD. The severity of GVHD was assessed with a clinical GVHD scoring system as described previously (20). In brief, mice were individually scored every week for five clinical parameters on a scale from zero to two: weight loss, posture, activity, fur, and skin. A clinical GVHD index was generated by summation of the five criteria scores (0–10). Survival was monitored daily. Animals with scores >5 were considered moribund and were killed. GVHD organ pathology for bowel (terminal ileum and ascending colon) and liver was assessed in a blinded fashion on formalin-preserved, paraffin-embedded, hematoxylin and eosin–stained histopathology sections with a semi-quantitative scoring system. In brief, bowel and liver were scored for 18–22 parameters associated with GVHD as described previously (21, 22).

CFSE Labeling. Cells were labeled with CFSE as described previously (23). In brief, T cells were incubated with CFSE at a final concentration of 2.5 μM in PBS at 37°C for 20 min. Cells were washed three times with PBS before i.v. injection.

Flow Cytometric Analysis. T cells were washed in FACS® buffer (PBS with 2% FBS and 0.1% sodium azide) and incubated for 15 min at 4°C with anti-CD16/CD32 FcR block. Subsequently, cells were incubated for 30 min at 4°C with antibodies and washed twice with FACS® buffer. Stained cells were resuspended in FACS® buffer and analyzed on a FACSCalibur™ flow cytometer (Becton Dickinson) with CELLQuest™ or Flowjo software (Treestar). For annexin V analysis, after cell surface staining, the stained cells were resuspended in 100 μl annexin V binding buffer and 5 μl annexin V Ab. After a 20-min incubation at room temperature in the dark, an additional 300 μl annexin V binding buffer was added, and the cells were analyzed.

ELISA. MLR supernatant IL-2 and IFNγ levels were performed according to the manufacturer's instructions with Quantikine M kits from R&D Systems.

DTA-1 Administration. For GVHD studies, DTA-1 and rat isotype control was administered by i.p. at days −1, 6, and 13 (1 mg/day). For adoptive transfer experiments with CFSE-labeled T cells, the antibodies were administered at day −1 (1 mg i.p.).

Online Supplemental Material. The opposite effects of GITR stimulation on $CD4^+CD25^-$ and $CD8^+CD25^-$ T cells remain even at different concentrations of DTA-1 Ab and are independent from the TNF–TNFR pathway. Supernatants from $CD4^+CD25^-$ T cells activated in the presence of GITR stimulation have decreased levels of IL-2 and IFNγ. Online supplemental material is available at http://www.jem.org/cgi/content/full/jem.20040116/DC1.

Results

Alloreactive $CD4^+$ and $CD8^+$ T Cells Up-regulate GITR. To assess whether activation of $CD4^+$ and $CD8^+$ T cells results in up-regulation of GITR expression, we analyzed GITR cell surface expression on activated (in vitro stimulation with anti-CD3 and anti-CD28 antibodies) and alloreactive (in vivo alloactivation after transfer into an allogeneic recipient) $CD4^+$ and $CD8^+$ T cells. In vitro stimulation with plate-bound anti-CD3/anti-CD28 antibodies of $CD4^+CD25^-$ and $CD8^+CD25^-$ T cells enhanced the expression of cell surface GITR, whereas freshly isolated immunoregulatory T cells had constitutive high levels of GITR (unpublished data). We used an MHC class I/II disparate model (C57BL/6→BALB/c) to analyze the expression of GITR on alloreactive T cells in vivo in two ways. First, we infused CFSE-labeled donor $CD3^+$ T cells into sublethally irradiated allogeneic and syngeneic recipients and recovered the cells from the spleen 3 d after infusion (Fig. 1 A). CFSE-labeled donor T cells from syngeneic recipients expressed low levels of cell surface GITR, in contrast with fast-dividing donor alloreactive T cells recovered from allogeneic recipients that had an activated phenotype ($CD25^+$ and $CD44^+$) and increased levels of GITR on their surface. Second, we infused T cell–depleted (TCD) allo-BM (C57BL/6 TCD-BM) and allogeneic T cells (C57BL/6) into lethally irradiated recipients (BALB/c), and after 9 d, determined the GITR expression on donor T cells from the spleens of these recipients (Fig. 1 B). We found that these (alloreactive) donor T cells indeed had an activated phenotype ($CD25^+$, $CD44^+$, and $CD62L^-$; unpublished data), and as expected, both $CD4^+$ and $CD8^+$ donor T cells had increased GITR expression. Therefore, we conclude that alloreactive $CD4^+$ and $CD8^+$ T cells up-regulate their GITR expression.

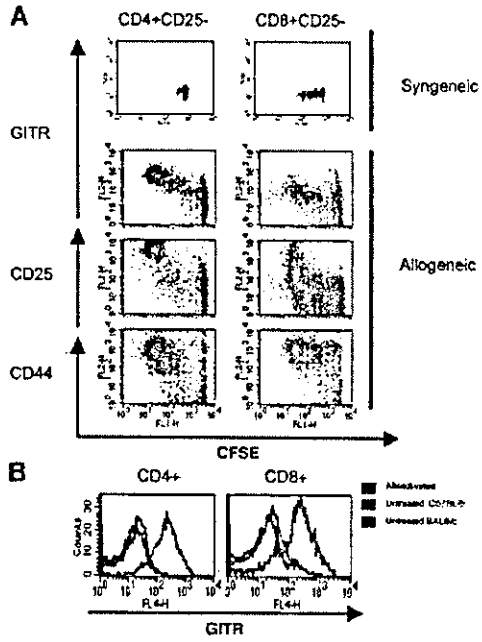

Figure 1. Alloactivation induces up-regulation of cell surface GITR on T cells. (A) Sublethally irradiated (750 cGy) syngeneic hosts (C57BL/6 Ly5.1) and allogeneic hosts (BALB/c) were infused with CFSE-labeled donor T cells (C57BL/6). GITR, CD25, and CD44 expression of these donor T cells was determined 3 d after infusion. (B) 9 d after BMT, GITR and CD25 expression was determined on splenic T cells from BALB/c recipients of C57BL/6 TCD-BM (5×10^6) and T cells (0.5×10^6), which were developing GVHD (red histogram). Blue histograms represent untransplanted controls (light blue, C57BL/6; dark blue, BALB/c).

Paradoxical Effect of GITR on $CD4^+CD25^-$ and $CD8^+CD25^-$ T Cells. We studied the effects of GITR stimulation on alloreactive T cells using an anti-GITR agonist mAb (DTA-1) for in vitro and in vivo experiments. To exclude the previously described effects of GITR on immunoregulatory T cells (15), we used purified C57BL/6 $CD4^+CD25^-$ and $CD8^+CD25^-$ T cells as effectors in MLR experiments with MHC class I/II disparate irradiated stimulators (BALB/c; Fig. 2 A). Addition of DTA-1 to the MLR resulted in an ~2-fold decrease in proliferation of $CD4^+CD25^-$ T cells, whereas $CD8^+CD25^-$ T cell proliferation increased by ~3.5-fold when compared with addition of control Ab (Fig. 2 A, top). To eliminate potentially confounding variables associated with GITR expression on immunoregulatory T cells, B cells, and macrophages present in the splenocyte population used as stimulators, splenocytes isolated from $GITR^{+/-}$ and $GITR^{-/-}$ mice were tested as stimulators. Because these mice are on a

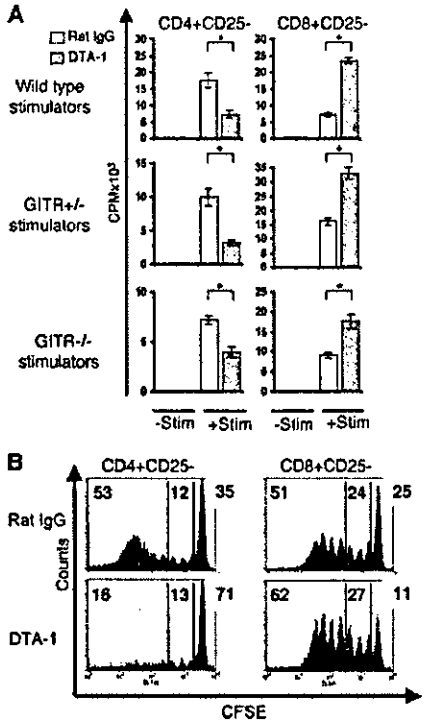

Figure 2. GITR stimulation induces paradoxical responses in $CD4^+$ $CD25^-$ and $CD8^+CD25^-$ T cells in vitro and in vivo. (A) An anti-GITR agonist Ab (DTA-1; 10 μg/ml) was added to MLRs of purified $CD4^+CD25^-$ and $CD8^+CD25^-$ splenic T cells as effector cells (10^5) with irradiated splenocytes as stimulators (2×10^5). (Wild-type stimulators) C57BL/6 effectors and BALB/c stimulators. ($GITR^{+/-}$ and $GITR^{-/-}$ stimulators) BALB/c effectors and $GITR^{+/-}$ or $GITR^{-/-}$ stimulators (C57BL/6 × 129/SvJ). −Stim, without stimulators. +Stim, with stimulators. *, $P < 0.001$. (B) Proliferative profile of recovered CFSE-labeled $CD4^+CD25^-$ and $CD8^+CD25^-$ T cells from sublethally irradiated hosts treated with 10 μg/ml DTA-1 or rat IgG control. These data are representative of three independent experiments. (top left) Percentage of alloreactive fast-proliferating donor T cells. (center) Percentage of slow proliferating donor T cells. (top right) Nondividing donor T cells.

mixed $H2^b$ background (C57BL/6 × 129/SvJ), we used purified $CD4^+CD25^-$ and $CD8^+CD25^-$ T cells from BALB/c mice as effectors (Fig. 2 A, bottom). Again, $CD4^+$ $CD25^-$ T cells showed decreased proliferation, whereas $CD8^+CD25^-$ T cell proliferation was enhanced by the addition of the DTA-1 Ab. Because this effect was observed using $GITR^{-/-}$ stimulators, we conclude that GITR stimulation via DTA-1 is independent of GITR expression on the stimulator population (including immunoregulatory T cells) and has a direct effect on $CD4^+CD25^-$ and $CD8^+CD25^-$ effector T cells. Also, this effect was not strain specific because results generated from T cells derived from C57BL/6 and BALB/c were consistent.

Our experiments clearly show inhibition of $CD4^+$ $CD25^-$ proliferation upon GITR stimulation, whereas other groups show enhancement of $CD4^+CD25^-$ T cell proliferation. Shimizu et al. (15) demonstrated that $CD4^+CD25^-$ T cells from $CD28^{-/-}$ were able to proliferate when stimulated via GITR. Tone et al. (11) showed that stimulation of GITR using a recombinant mouse GITRL could increase the proliferation of a Th2 clone through a wide range of cognate peptide concentration and a Th1 clone only at low peptide concentrations. Therefore, we analyzed whether the difference in proliferation of the alloreactive T cells could depend on the amount of anti-GITR agonist Ab present in the MLR. Because the Ag concentration is fixed (allorecognition), we titrated the anti-GITR Ab concentration over a 4-log range (Fig. S1, available at http://www.jem.org/cgi/content/full/jem.20040116/DC1). Addition of different concentrations spanning from 0.01 to 10 μg/ml of the GITR-stimulating Ab (DTA-1) to an MLR resulted again in decreased proliferation of $CD4^+CD25^-$ T cells and increased $CD8^+$ $CD25^-$ T cell proliferation.

Our data would suggest that $CD4^+CD25^-$ T cells from $GITR^{-/-}$ mice would show increased proliferation, whereas $CD8^+CD25^-$ T cells from $GITR^{-/-}$ mice would have impaired proliferative capacity. Ronchetti et al. (17) have shown that, indeed, upon anti-CD3 stimulation, $CD4^+$ but not the $CD8^+$ $GITR^{-/-}$ subpopulation had a higher proliferation rate than the $CD4^+$ $GITR^{+/+}$ subpopulation. Because T cell responses to Ab stimulation may be irrelevant to our model of allo-BMT, we tested the proliferative capacity of $GITR^{-/-}$ and $GITR^{+/-}$ T cells derived from mice of a mixed background (C57BL/6 × 129/SvJ). Our preliminary results indicate that there is no difference in $CD4^+CD25^-$ and $CD8^+CD25^-$ T cell proliferation upon allostimulation using third party stimulators (BALB/c; unpublished data). However, these experiments were performed with cells from $GITR^{-/-}$ and $GITR^{+/-}$ on a mixed background and we cannot rule out that genetic differences (other than the presence or absence of GITR) could have affected the alloresponse. Therefore, definitive experiments will have to be deferred until the $GITR^{-/-}$ mice have been completely backcrossed (>N 10).

To test whether the in vitro effects of anti-GITR agonist Ab (DTA-1) on alloreactive T cells were consistent in vivo, sublethally irradiated BALB/c mice were treated with DTA-1 or rat IgG control before adoptive transfer of C57BL/6 CFSE-labeled $CD4^+CD25^-$ or $CD8^+CD25^-$ T cells (Fig. 2 B). 3 d after T cell infusion, donor T cells were recovered and analyzed by flow cytometry. The in vivo proliferation profile of CFSE-labeled T cells allows the discrimination of slow proliferating cells, described in some models as homeostatic expansion, versus fast-dividing alloreactive T cells (24). GITR stimulation had no impact on the proportion of slow dividing $CD4^+CD25^-$ (12% in controls vs. 13% in DTA-1–treated recipients) and $CD8^+CD25^-$ (24 vs. 27%) T cells. However, GITR stimulation decreased the percentage of fast-dividing alloreactive $CD4^+CD25^-$ T cells (from 53 to 16%) and increased the percentage of fast-dividing alloreactive $CD8^+CD25^-$ T cells (from 51 to 62%). There were more nondividing $CD4^+CD25^-$ T cells in the DTA-1–treated group (71% in DTA-1–treated recipients vs. 35% in the controls), and

fewer nondividing $CD8^+CD25^-$ T cells in the DTA-1–treated group (11 vs. 25%) compared with the control Ab groups. These results indicate that GITR stimulation in vivo can inhibit alloreactive $CD4^+CD25^-$ expansion while it enhances alloreactive $CD8^+CD25^-$ expansion.

Fas–FasL Mediate GITR Inhibition of $CD4^+CD25^-$ T Cell Expansion. To determine if the Fas–FasL pathway was involved in GITR inhibition of $CD4^+CD25^-$ expansion, we studied the effect of GITR stimulation on cell surface expression of Fas and FasL (Fig. 3 A). $CD4^+CD25^-$ and $CD8^+CD25^-$ T cells allostimulated in the presence of the agonistic anti-GITR Ab (DTA-1) did not increase Fas expression nor was there a difference in FasL expression (unpublished data), although FasL cell surface expression is notoriously difficult to demonstrate by flow cytometric analysis. To address this question in a different assay, we studied the effect of DTA-1 on T cells from Fas-deficient *lpr* mice (Fig. 3 B). Addition of DTA-1 to an MLR had no effect on proliferation by *lpr* $CD4^+CD25^-$ T cells, in contrast with the inhibitory effect on wild-type $CD4^+CD25^-$ T cells. Alloreactive proliferation of both wild-type and *lpr* $CD8^+CD25^-$ T cells was increased when DTA-1 was added to the MLR. To demonstrate that GITR inhibition of $CD4^+CD25^-$ proliferation was due to FasL signaling, we studied the effect of anti-FasL blocking Ab during allostimulation (Fig. 3 C). As aforementioned, $CD4^+CD25^-$ T cell proliferation was impaired in the presence of DTA-1 while the addition of the FasL blocking Ab rescued $CD4^+CD25^-$ proliferation, although not completely. Because $CD4^+CD25^-$ proliferation is not completely restored after FasL blocking, other members of the TNFR family could be implicated. Proliferation of purified $CD4^+CD25^-$ T cells from $TNF^{-/-}$ and $TRAIL^{-/-}$ mice allostimulated in the presence of DTA-1 treatment remained impaired (Fig. 3 D). We further tested the role of TNFR1 by using an anti-TNFR1 blocking Ab. Proliferation of purified $CD4^+CD25^-$ T cells with TNFR1 and TNF blocking Ab in the presence of GITR stimulation still remained impaired (Fig. S2, available at http://www.jem.org/cgi/content/full/jem.20040116/DC1). These results show that GITR-mediated inhibition of $CD4^+CD25^-$ T cell expansion involves the Fas–FasL pathway and not the TNFR or TRAIL pathways, although the involvement of other members of the TNF family cannot be excluded.

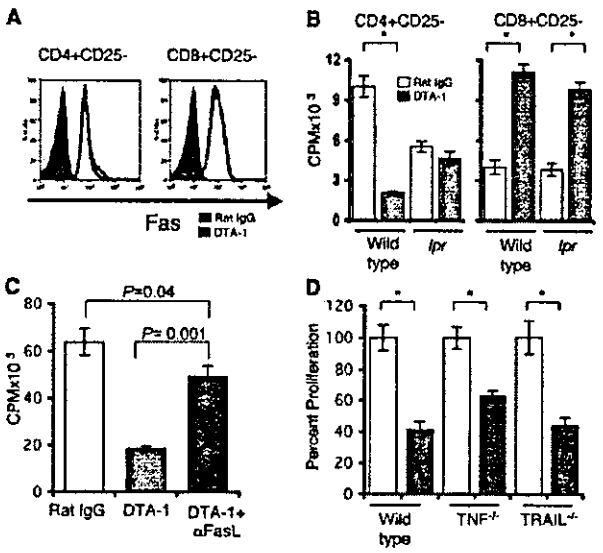

Figure 3. Fas–FasL pathway is involved in inhibition of $CD4^+CD25^-$ proliferation. (A) Fas expression was determined on purified C57BL/6 $CD4^+CD25^-$ and $CD8^+CD25^-$ T cells 72 h after anti-GITR agonist Ab (DTA-1) was added to MLRs with irradiated BALB/c stimulators. (shaded histograms) Isotype control. (blue histograms) Rat IgG–treated MLR. (red histograms) DTA-1–treated MLR. (B) DTA-1 was added to MLRs with purified $CD4^+CD25^-$ and $CD8^+CD25^-$ from *lpr* (B6.MRL-*Fas*^{lpr}) or wild-type (C57BL/6) mice as effectors and irradiated BALB/c splenocytes as stimulators. These data are representative of three experiments. *, $P < 0.001$. (C) Purified C57BL/6 $CD4^+CD25^-$ T cells were stimulated with irradiated BALB/c splenocytes in the presence of rat IgG control Ab, DTA-1 Ab, or DTA-1 plus MFL3, a FasL-blocking Ab. These data are representative of two independent experiments. (D) $CD4^+CD25^-$ T cells were purified from wild-type C57BL/6, C57BL/6-$TNF^{-/-}$, and C57BL/6 $TRAIL^{-/-}$ mice and stimulated with irradiated BALB/c splenocytes in the presence of rat IgG control Ab or DTA-1 Ab. (unshaded bars) Rat IgG treatment. (shaded bars) DTA-1 treatment. Results are presented as percent proliferation and are representative of two independent experiments. *, $P < 0.007$.

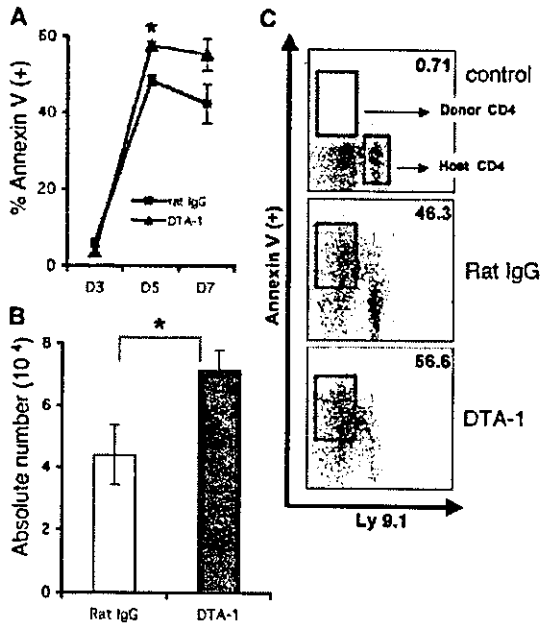

Figure 4. GITR stimulation induces early apoptosis of $CD4^+CD25^-$ alloreactive T cells after BMT. Lethally irradiated (900 cGy) BALB/c recipients of C57BL/6 TCD-BM and C57BL/6 $CD4^+CD25^-$ splenic T cells were treated with DTA-1 or control Ab (1 mg i.p. on days −1 and 6). Spleens were harvested on days 3, 5, and 7, and stained for annexin V (+) cells ($n = 3$ per group, per time point). (A) Time course of the percentage of donor-derived annexin V (+) cells is shown. *, $P = 0.0004$. (B) Absolute numbers of annexin V (+) donor $CD4^+$ T cells at day 5. *, $P = 0.05$. (C) Representative FACS® analyses of annexin V (+) donor and host $CD4^+$ T cells at day 7.

We measured the amount of IL-2 production of $CD4^+CD25^-$ T cells in the presence or absence of DTA-1 during allostimulation (Fig. S3, available at http://www.jem.org/cgi/content/full/jem.20040116/DC1). IL-2 was decreased in MLR supernatants of DTA-1–treated cocultures compared with control Ab–treated cocultures at days 2 and 5 of coculture (day 2, ~1.5 fold decrease and day 5, ~2.1-fold decrease). These decreased levels of IL-2 detected in our system may be a reflection of less viable $CD4^+CD25^-$ T cells.

These experiments indicate that GITR activation can initiate Fas-mediated AICD of alloreactive $CD4^+CD25^-$ T cells, whereas GITR stimulation of $CD8^+CD25^-$ T cell proliferation is independent of Fas–FasL signaling.

In Vivo GITR Stimulation Increases Apoptosis of $CD4^+$ $CD25^-$ Alloreactive T Cells. We wanted to address in our GVHD model if GITR stimulation increased $CD4^+CD25^-$ apoptosis in vivo. We infused 3×10^6 purified $CD4^+CD25^-$ T cells into lethally irradiated hosts treated with DTA-1 or rat IgG control Ab and determined apoptosis of donor T cells after 3, 5, and 7 d of allo-BMT (Fig. 4 A). Donor $CD4^+CD25^-$ T cells harvested from spleens of DTA-1–treated recipients showed increased annexin V staining when compared with donor T cells derived from control recipients treated with rat IgG (Fig. 4, B and C). We also studied the expression of activation markers at day 7 after BMT on $CD4^+CD25^-$ T cells from the DTA-1–treated group compared with the rat IgG–treated group and detected no significant difference in the level of CD25 and CD44 expression (unpublished data). These results indicate that DTA-1 treatment induces significantly more apoptosis of donor alloreactive $CD4^+CD25^-$ T cells early in the course of GVHD.

GITR Stimulation Modulates GVHD. In the C57BL/6→BALB/c strain combination, alloreactive $CD4^+$ T cells are more potent as GVHD effectors (25), whereas graft-versus-tumor activity is mostly dependent on alloreactive $CD8^+$ T cells (26). We used this model to determine the effects of anti-GITR agonistic Ab (DTA-1) on alloreactive $CD4^+CD25^-$ and $CD8^+CD25^-$ T cells during the development of GVHD. Pilot experiments determined that DTA-1 administration beginning at day −1 was optimal. The dose and schedule were consistent with previous papers in which anti-GITR antibodies have been used in vivo (weekly administration of 1 mg i.p.; references 16, 27).

We hypothesized that DTA-1 administration to allo-BMT recipients could ameliorate GVHD mediated by $CD4^+CD25^-$ T cells due to enhanced AICD of alloreactive T cells and aggravate GVHD mediated by $CD8^+CD25^-$ T cells due to their enhanced proliferation by GITR stimulation. Indeed, we observed that DTA-1–treated recipients of $CD4^+CD25^-$ C57BL/6 donor T cells, although not free of disease, had a significant delay and decrease in GVHD morbidity and mortality compared with recipients treated with a control Ab (Fig. 5, left).

Although alloreactive $CD4^+CD25^-$ cells are more potent on a per cell basis in the C57BL/6→BALB/c model,

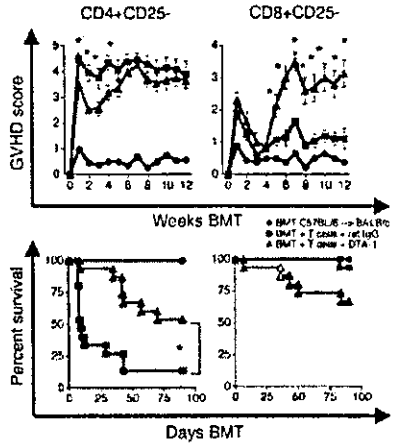

Figure 5. GITR stimulation decreases GVHD mediated by $CD4^+CD25^-$ cells and increases GVHD mediated by $CD8^+CD25^-$ T cells. Lethally irradiated (900 cGy) BALB/c recipients of C57BL/6 TCD-BM and C57BL/6 $CD4^+CD25^-$ or $CD8^+CD25^-$ splenic T cells were treated with DTA-1 Ab (1 mg i.p. on days −1, 6, and 13) or control Ab. (top) Mean ± SEM clinical GVHD scores. (bottom) Kaplan-Meier survival curves. Data shown are combined from three experiments, $n = 15$ per group. *, $P \leq 0.01$.

this strain combination has a class I and class II disparity, and $CD8^+CD25^-$ can induce GVHD. In other GVHD models with full MHC disparity, $CD8^+$-mediated GVHD can always be demonstrated (28). DTA-1–treated recipients of donor BM and donor $CD8^+CD25^-$ T cells had significantly increased GVHD morbidity and mortality (Fig. 5, right). Additional experiments in a MHC-matched strain combination in which GVHD is primarily dependent on alloreactive $CD8^+$ T cells (B10.BR→CBA/J) demonstrated that DTA-1 administration to allo-BMT recipients could aggravate GVHD (unpublished data). However, these mice were infused with unfractionated donor splenocytes; thus, increased mortality could also be due to the inhibition of suppressor function via GITR stimulation (15, 16) independent of its effect on $CD8^+$ donor T cells.

To further assess GVHD, target organ histopathology was studied (Fig. 6). Mice transplanted and infused with donor $CD4^+CD25^-$ donor T cells were killed at day 21 (Fig. 6 A). We lowered the dose of donor $CD4^+CD25^-$ T cells to 0.3×10^6 and delayed the time of organ harvest to day 21 due to high mortality in the rat IgG control group (Fig. 5). We observe significantly less GVHD target organ damage in liver and intestines of DTA-1–treated recipients compared with control recipients of $CD4^+CD25^-$ T cells. There was greater thymic cellularity in DTA-1–treated recipients, which is consistent with less thymi damage. Also, higher numbers of granulocytes were detected, consistent with less GVHD-associated myelosuppression. Mice transplanted and infused with $CD8^+CD25^-$ donor T cells were killed, and organs were harvested at day 55, when differences in clinical scores were more pronounced (Fig. 6 B). Consistent with our previous results, GITR stimulation of

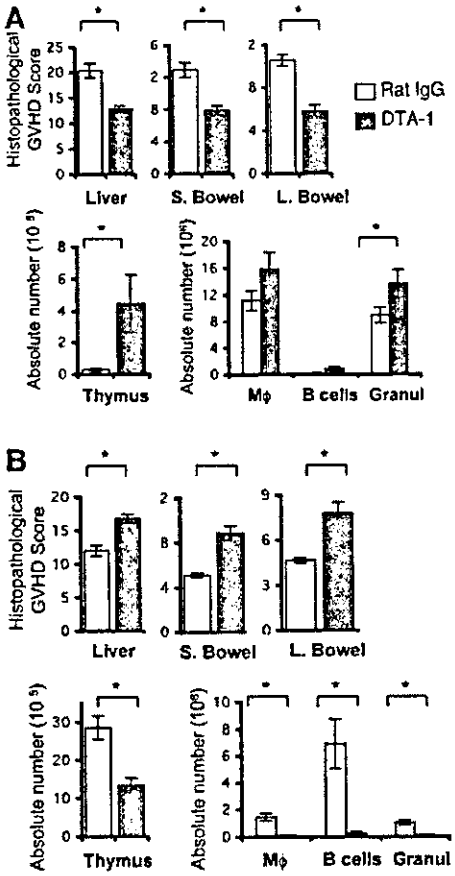

Figure 6. GITR stimulation decreases GVHD-associated organ damage mediated by $CD4^+CD25^-$ T cells and increases GVHD-associated organ damage mediated by $CD8^+CD25^-$ T cells. Lethally irradiated (900 cGy) BALB/c recipients of C57BL/6 TCD-BM and C57BL/6 $CD4^+CD25^-$ cells or $CD8^+CD25^-$ splenic T cells were treated with DTA-1 Ab or control Ab (1 mg i.p. on days −1, 6, and 13). Recipients of $CD4^+CD25^-$ T cells were killed, and organs were harvested on day 21 (A). Recipients of $CD8^+CD25^-$ T cells were killed, and organs were harvested on day 55 (B). (top) A semi-quantitative histopathological analysis for GVHD in liver, small bowel, and large bowel. (bottom left) The absolute number of thymocytes. (bottom right) The absolute numbers of splenic Mac-1^+ (Mϕ), B cells, and granulocytes (Granul) were analyzed by flow cytometry. Data shown are representative of one experiment, $n = 9$–10 per group. *, $P \leq 0.05$.

donor $CD8^+CD25^-$ donor T cells resulted in increased target organ damage and myelosuppression.

Discussion

Previous experiments have indicated that in vitro stimulation of GITR on immunoregulatory T cells inhibits their suppressive effect and that in vivo GITR stimulation induced development of autoimmunity presumably due to immunoregulatory T cell inhibition (15, 16). The effects of GITR stimulation on $CD4^+$ and $CD8^+$ have not been fully addressed, especially in vivo. Here, we demonstrate that GITR stimulation in vitro and in vivo has an important role in the costimulation of alloreactive $CD4^+CD25^-$ and $CD8^+CD25^-$ T cells independent of its effect on immunoregulatory T cells. Stimulation with a GITR-activating Ab inhibited $CD4^+CD25^-$ proliferation and decreased GVHD, whereas it enhanced alloreactive $CD8^+CD25^-$ T cell proliferation and increased GVHD. Our data indicate that GITR-mediated inhibition of $CD4^+CD25^-$ T cell expansion involves the Fas–FasL pathway, suggesting that GITR activation can initiate Fas-mediated AICD of alloreactive $CD4^+CD25^-$ T cells, whereas GITR stimulation of $CD8^+CD25^-$ T cell proliferation is independent of Fas–FasL signaling. Our results are consistent with the notion that GITR stimulation could lower the threshold for T cell activation inducing increased AICD in $CD4^+CD25^-$, but not in $CD8^+CD25^-$ T cells, where it induces proliferation. Thus, GITR stimulation of alloreactive $CD4^+CD25^-$ T cells in vivo can provide a novel strategy to prevent or treat GVHD.

Other laboratories have described GITR signaling as costimulatory for CD4 and CD8 (15, 17). Experiments using polyclonal stimulation with low concentrations of plate-bound or soluble anti-CD3 Ab (0.1–0.5 μg/ml; references 15, 17, 18) demonstrate that anti-GITR increases proliferation, but in some experiments, this costimulation is lost at higher concentrations of anti-CD3 Ab (1–3 μg/ml; references 15, 18). Our experiments addressing the role of GITR stimulation using Ab stimulation showed no difference in the proliferation of $CD4^+CD25^-$ cells stimulated with 10 μg/ml of soluble anti-CD3 and soluble anti-GITR agonistic Ab (DTA-1). $CD8^+CD25^-$ T cell proliferation under the same conditions was slightly increased (unpublished data). However, experiments addressing the effects of GITR stimulation upon Ag-specific recognition, a more representative model of allo-specific responses, show results consistent with ours. Because GVHD is a Th1-mediated complication of BMT (29, 30), experiments by Tone et al. (11) with a Th1 clone derived from TCR transgenic mice using a rGITRL for GITR stimulation are more relevant to our model. When the Th1 clone is stimulated with a low concentration of the cognate peptide (1 nM), rGITRL proliferation is enhanced. In contrast, when the Th1 clone is stimulated in the presence of rGITRL and higher peptide concentrations (10–100 nM), proliferation is inhibited. The same results were observed using naive T cells derived from the same transgenic mice where the presence of GITR stimulation at high peptide concentrations inhibited proliferation (11).

Furthermore, Shimizu et al. (15) have shown that xenostimulated $CD4^+CD25^-$ T cells have decreased proliferation in the presence of anti-GITR agonistic Ab (DTA-1). Murine $CD4^+CD25^-$ T cells were stimulated with rat APCs. The authors demonstrate that DTA-1 has no cross-reactivity with rat APCs, indicating that any effect observed by the addition of the agonist Ab will be a result of its direct effect on the murine cells. When $CD4^+CD25^-$ T cells were xenostimulated in the presence of a control Ab, they proliferate extensively, whereas addition of DTA-1 to the same culture resulted in a marked decrease in proliferation.

These experiments that analyze Ag-dependent T cell activation are very similar to our results, suggesting that during allo- and xenostimulation the addition of GITR stimulation may induce a potent costimulation, which can inhibit proliferation at higher Ag concentration. Our experiments indicate that this inhibitory effect on proliferation could be due to AICD.

We believe that the overall effect of in vivo GITR stimulation needs to be reconsidered because GITR stimulation can have a differential and/or paradoxical effect on regulatory T cells, $CD4^+$ effector T cells, and $CD8^+$ effector T cells. Our data in clinically relevant models for GVHD suggest that in vivo GITR stimulation holds therapeutic promise for the separation of CD8-mediated graft-versus-tumor activity from CD4-mediated GVHD activity.

S.J. Muriglan would like to dedicate this paper to Donald Holmquist.

A.N. Houghton and T. Ramirez-Montagut were supported by the National Institutes of Health (grants CA59350, CA58621, and CA33049) and Swim Across America. This work was supported by RO1 grants HL69929 and HL72412 from the National Institutes of Health (to M.R.M. van den Brink). M.R.M. van den Brink is the recipient of a Damon Runyon Scholar Award of the Cancer Research Fund.

Submitted: 20 January 2004
Accepted: 28 May 2004

References

1. Nocentini, G., L. Giunchi, S. Ronchetti, L.T. Krausz, A. Bartoli, R. Moraca, G. Migliorati, and C. Riccardi. 1997. A new member of the tumor necrosis factor/nerve growth factor receptor family inhibits T cell receptor-induced apoptosis. *Proc. Natl. Acad. Sci. USA.* 94:6216–6221.
2. Nocentini, G., A. Bartoli, S. Ronchetti, L. Giunchi, A. Cupelli, D. Delfino, G. Migliorati, and C. Riccardi. 2000. Gene structure and chromosomal assignment of mouse GITR, a member of the tumor necrosis factor/nerve growth factor receptor family. *DNA Cell Biol.* 19:205–217.
3. Gurney, A.L., S.A. Marsters, R.M. Huang, R.M. Pitti, D.T. Mark, D.T. Baldwin, A.M. Gray, A.D. Dowd, A.D. Brush, A.D. Heldens, et al. 1999. Identification of a new member of the tumor necrosis factor family and its receptor, a human ortholog of mouse GITR. *Curr. Biol.* 9:215–218.
4. Kwon, B., K.Y. Yu, J. Ni, G.L. Yu, I.K. Jang, Y.J. Kim, L. Xing, D. Liu, S.X. Wang, and B.S. Kwon. 1999. Identification of a novel activation-inducible protein of the tumor necrosis factor receptor superfamily and its ligand. *J. Biol. Chem.* 274:6056–6061.
5. Spinicelli, S., G. Nocentini, S. Ronchetti, L.T. Krausz, R. Bianchini, and C. Riccardi. 2002. GITR interacts with the pro-apoptotic protein Siva and induces apoptosis. *Cell Death Differ.* 9:1382–1384.
6. Nocentini, G., S. Ronchetti, A. Bartoli, S. Spinicelli, D. Delfino, L. Brunetti, G. Migliorati, and C. Riccardi. 2000. Identification of three novel mRNA splice variants of GITR. *Cell Death Differ.* 7:408–410.
7. Shin, H.H., M.H. Lee, S.G. Kim, Y.H. Lee, B.S. Kwon, and H.S. Choi. 2002. Recombinant glucocorticoid induced tumor necrosis factor receptor (rGITR) induces NOS in murine macrophage. *FEBS Lett.* 514:275–280.
8. Shin, H.H., B.S. Kwon, and H.S. Choi. 2002. Recombinant glucocorticoid induced tumour necrosis factor receptor (rGITR) induced COX-2 activity in murine macrophage Raw 264.7 cells. *Cytokine.* 19:187–192.
9. Lee, H.S., H.H. Shin, B.S. Kwon, and H.S. Choi. 2003. Soluble glucocorticoid-induced tumor necrosis factor receptor (sGITR) increased MMP-9 activity in murine macrophage. *J. Cell. Biochem.* 88:1048–1056.
10. Shin, H.H., H.W. Lee, and H.S. Choi. 2003. Induction of nitric oxide synthase (NOS) by soluble glucocorticoid induced tumor necrosis factor receptor (sGITR) is modulated by IFN-gamma in murine macrophage. *Exp. Mol. Med.* 35:175–180.
11. Tone, M., Y. Tone, E. Adams, S.F. Yates, M.R. Frewin, S.P. Cobbold, and H. Waldmann. 2003. Mouse glucocorticoid-induced tumor necrosis factor receptor ligand is costimulatory for T cells. *Proc. Natl. Acad. Sci. USA.* 100:15059–15064.
12. Ronchetti, S., G. Nocentini, C. Riccardi, and P.P. Pandolfi. 2002. Role of GITR in activation response of T lymphocytes. *Blood.* 100:350–352.
13. Yu, K.Y., H.S. Kim, S.Y. Song, S.S. Min, J.J. Jeong, and B.S. Youn. 2003. Identification of a ligand for glucocorticoid-induced tumor necrosis factor receptor constitutively expressed in dendritic cells. *Biochem. Biophys. Res. Commun.* 310:433–438.
14. Kim, J.D., B.K. Choi, J.S. Bae, U.H. Lee, I.S. Han, H.W. Lee, B.S. Youn, D.S. Vinay, and B.S. Kwon. 2003. Cloning and characterization of GITR ligand. *Genes Immun.* 4:564–569.
15. Shimizu, J., S. Yamazaki, T. Takahashi, Y. Ishida, and S. Sakaguchi. 2002. Stimulation of CD25(+)CD4(+) regulatory T cells through GITR breaks immunological self-tolerance. *Nat. Immunol.* 3:135–142.
16. Uraushihara, K., T. Kanai, K. Ko, T. Totsuka, S. Makita, R. Iiyama, T. Nakamura, and M. Watanabe. 2003. Regulation of murine inflammatory bowel disease by CD25+ and CD25-CD4+ glucocorticoid-induced TNF receptor family-related gene+ regulatory T cells. *J. Immunol.* 171:708–716.
17. Ronchetti, S., O. Zollo, S. Bruscoli, M. Agostini, R. Bianchini, G. Nocentini, E. Ayroldi, and C. Riccardi. 2004. GITR, a member of the TNF receptor superfamily, is costimulatory to mouse T lymphocyte subpopulations. *Eur. J. Immunol.* 34:613–622.
18. Kohm, A.P., J.S. Williams, and S.D. Miller. 2004. Cutting edge: ligation of the glucocorticoid-induced TNF receptor enhances autoreactive CD4(+) T cell activation and experimental autoimmune encephalomyelitis. *J. Immunol.* 172:4686–4690.
19. Alpdogan, O., S.J. Muriglan, B.J. Kappel, E. Doubrovina, C. Schmaltz, R. Schiro, J.M. Eng, A.S. Greenberg, L.M. Willis, J.A. Rotolo, et al. 2003. Insulin-like growth factor-I enhances lymphoid and myeloid reconstitution after allogeneic bone marrow transplantation. *Transplantation.* 75:1977–1983.
20. Cooke, K.R., L. Kobzik, T.R. Martin, J. Brewer, J. Delmonte, Jr., J.M. Crawford, and J.L. Ferrara. 1996. An experimental model of idiopathic pneumonia syndrome after bone marrow transplantation: I. The roles of minor H antigens and endotoxin. *Blood.* 88:3230–3239.
21. Crawford, J.M. 1997. Graft-versus-host disease of the liver. *In* Graft-vs.-Host Disease. J.L.M. Ferrara, H.J. Deeg, and S.J. Burakoff, editors. Marcel Dekker, New York. 315–336.
22. Hill, G.R., J.M. Crawford, K.R. Cooke, Y.S. Brinson, L. Pan, and J.L. Ferrara. 1997. Total body irradiation and acute graft-versus-host disease: the role of gastrointestinal damage and inflammatory cytokines. *Blood.* 90:3204–3213.

23. Lyons, A.B., and C.R. Parish. 1994. Determination of lymphocyte division by flow cytometry. *J. Immunol. Methods.* 171:131–137.
24. Alpdogan, O., S.J. Muriglan, J.M. Eng, L.M. Willis, A.S. Greenberg, B.J. Kappel, and M.R. van den Brink. 2003. IL-7 enhances peripheral T cell reconstitution after allogeneic hematopoietic stem cell transplantation. *J. Clin. Invest.* 112: 1095–1107.
25. Hoffmann, P., J. Ermann, M. Edinger, C.G. Fathman, and S. Strober. 2002. Donor-type $CD4^+CD25^+$ regulatory T cells suppress lethal acute graft-versus-host disease after allogeneic bone marrow transplantation. *J. Exp. Med.* 196:389–399.
26. Edinger, M., P. Hoffmann, J. Ermann, K. Drago, C.G. Fathman, S. Strober, and R.S. Negrin. 2003. CD4+CD25+ regulatory T cells preserve graft-versus-tumor activity while inhibiting graft-versus-host disease after bone marrow transplantation. *Nat. Med.* 9:1144–1150.
27. Shimizu, J., and E. Moriizumi. 2003. CD4+CD25− T cells in aged mice are hyporesponsive and exhibit suppressive activity. *J. Immunol.* 170:1675–1682.
28. Schmaltz, C., O. Alpdogan, K.J. Horndasch, S.J. Muriglan, B.J. Kappel, T. Teshima, J.L. Ferrara, S.J. Burakoff, and M.R. van den Brink. 2001. Differential use of Fas ligand and perforin cytotoxic pathways by donor T cells in graft-versus-host disease and graft-versus-leukemia effect. *Blood.* 97:2886–2895.
29. Krenger, W., and J.L. Ferrara. 1996. Graft-versus-host disease and the Th1/Th2 paradigm. *Immunol. Res.* 15:50–73.
30. Krenger, W., G.R. Hill, and J.L. Ferrara. 1997. Cytokine cascades in acute graft-versus-host disease. *Transplantation.* 64: 553–558.

ARTHRITIS & RHEUMATISM
Vol. 50, No. 8, August 2004, pp 2450–2458
DOI 10.1002/art.20367

Induction of RANKL Expression and Osteoclast Maturation by the Binding of Fibroblast Growth Factor 2 to Heparan Sulfate Proteoglycan on Rheumatoid Synovial Fibroblasts

Kazuhisa Nakano, Yosuke Okada, Kazuyoshi Saito, and Yoshiya Tanaka

Objective. **Rheumatoid arthritis (RA) is characterized by progressive joint destruction. The aim of this study was to clarify the relevance of RA synovial fibroblasts (RASFs) and fibroblast growth factor 2 (FGF-2), which is produced abundantly by RASFs, to the osteoclastogenesis and bone resorption in RA.**

Methods. **Synovial fibroblasts were prepared from the synovial tissues of 10 patients with active RA and 7 patients with osteoarthritis (OA). The expression of RANKL, intercellular adhesion molecule 1 (ICAM-1), FGF receptor 1 (FGFR-1), and heparan sulfate proteoglycan (HSPG) on synovial fibroblasts was measured by FACScan. Osteoclast formation in cocultures of RASFs and peripheral blood mononuclear cells (PBMCs) was evaluated by tartrate-resistant acid phosphatase staining and a pit-formation assay using dentin slices.**

Results. **FGF-2 induced the expression of both RANKL and ICAM-1 on RASFs more so than on OA synovial fibroblasts (OASFs). FGF-2–induced up-regulation of RANKL and ICAM-1 was inhibited by anti–FGF-2 antibody. Although FGFR-1 was equally expressed on RASFs and OASFs, HSPG was highly expressed on RASFs. Up-regulation of RANKL by FGF-2 on RASFs was diminished by the removal of heparan sulfate with heparitinase. Osteoclast formation from PBMCs induced by RASFs was inhibited by the addition of either heparitinase, anti–ICAM-1 antibody, anti–FGF-2 antibody, or osteoprotegerin. FGF-2–induced RANKL on RASFs and osteoclast formation were suppressed by an inhibitor of ERK.**

Conclusion. **FGF-2 was transferred to FGFR-1 through binding to HSPG, which is characteristically expressed on RASFs, resulting in RANKL- and ICAM-1–mediated maturation of osteoclasts via ERK activation. Thus, we propose that FGF-2 not only augments the proliferation of RASFs, but also is involved in osteoclast maturation, which leads to bone destruction in RA.**

Rheumatoid arthritis (RA) is an autoimmune disease characterized by progressive joint destruction that results from inflammation of multiple synovial joints. Destruction of bone and cartilage is one of the most serious problems in RA patients. Although histologic analyses have demonstrated that osteoclastic bone resorption at the bone–pannus interface is increased in RA joints (1), the mechanism has not yet been clarified. Since it has been reported that synovial cells from RA patients are capable of developing into osteoclasts (2), it is possible that the synovial tissue environment regulates osteoclastogenesis and results in joint destruction.

Fibroblast growth factor 2 (FGF-2) is a member of the family of heparin-binding cytokines with potent mitogenic effects on a variety of cells of mesodermal and ectodermal origin (3). FGF-2 has been reported to stimulate bone resorption in bone organ cultures (4), as well as osteoclastogenesis in a mouse bone marrow culture (5). Furthermore, it has been reported that among several bone-resorptive cytokines, only the FGF-2 concentration in the synovial fluid of RA patients was positively correlated with the severity of joint destruction (6). Recently, Yamashita et al (7) showed that

Kazuhisa Nakano, MD, Yosuke Okada, MD, Kazuyoshi Saito, MD, Yoshiya Tanaka, MD: University of Occupational and Environmental Health, Kitakyushu, Japan.

Address correspondence and reprint requests to Yoshiya Tanaka, MD, First Department of Internal Medicine, School of Medicine, University of Occupational and Environmental Health, 1-1 Iseigaoka Yahatanishi-ku, Kitakyushu, 807-8555 Japan. E-mail: tanaka@med.uoeh-u.ac.jp.

Submitted for publication June 18, 2003; accepted in revised form March 29, 2004.

anti–FGF-2–neutralizing antibody inhibited bone destruction in the joints of rats with adjuvant-induced arthritis, suggesting that the control of FGF-2 may prove to be therapeutically useful for RA. However, FGF-2 requires the presence of heparan sulfate proteoglycans (HSPGs) to bind FGF receptor (FGFR). HSPGs are coreceptors for FGF-2 and strongly promote the binding of FGF to FGFR and the subsequent activation of the receptor (8–10). Recent genetic studies in *Drosophila* provided compelling evidence that HSPGs are essential for FGF signaling in vivo (11).

The present study was designed to determine the role of FGF-2 and HSPG in the osteoclastogenesis that occurs in patients with RA. Our results showed that FGF-2/HSPG binding may provide powerful tools for inhibiting bone destruction in RA.

MATERIALS AND METHODS

Cell cultures. Synovial tissues were obtained from patients with active rheumatoid arthritis (12) and osteoarthritis (OA) (13), diagnosed according to the criteria of the American College of Rheumatology (formerly, the American Rheumatism Association), who were undergoing joint replacement surgery or synovectomy. Synovial tissues samples were dissected under sterile conditions in phosphate buffered saline (PBS), and immediately prepared for culture of fibroblast-like synovial cells.

Briefly, the tissue sample was minced into small pieces and digested with collagenase (Sigma-Aldrich Japan, Tokyo, Japan) in serum-free Dulbecco's modified Eagle's medium (DMEM; Gibco BRL, Grand Island, NY). After filtering through a nylon mesh, the cells were extensively washed, and suspended in DMEM, supplemented with 10% fetal calf serum (FCS; Bio-Pro, Karlsruhe, Germany). Finally, isolated cells were seeded in 25-cm^2 culture flasks (Falcon, Lincoln Park, NJ) and cultured in a humidified chamber with an atmosphere of 5% carbon dioxide. After overnight culture, nonadherent cells were removed, and incubation of adherent cells was continued in fresh medium. At confluence, the cells were trypsinized, passaged at a 1:3 split ratio, and recultured. The medium was changed twice each week, and the cells were used after 3–5 passages.

The study protocol was approved by the Ethics Review Committee of the University of Occupational and Environmental Health, School of Medicine. A signed consent form was obtained from each subject before tissue collection.

Reagents and monoclonal antibodies. FGF-2, osteoprotegerin (OPG) (PeproTech, London, UK), PD 98059, SB 202190 (both from Funakoshi, Tokyo, Japan), and chondroitinase ABC (Seikagaku, Tokyo, Japan) were purchased. Heparinase and heparitinase I and II were kindly donated by the Tokyo Research Institute of Seikagaku. Neutralizing antibodies against human FGF-2 produced in goats and nonimmune goat IgG were purchased from R&D Systems (Minneapolis, MN). The following monoclonal antibodies (mAb) were used as purified immunoglobulins in the preparation of synovial fibroblasts, staining, and analysis of cell surface molecules: anti–heparan sulfate mAb 10E4 (Seikagaku), anti-RANKL polyclonal antibody (C-20; Santa Cruz Biotechnology, Santa Cruz, CA), CD54 (ICAM-1) mAb 84H10 (kindly provided by S. Shaw, NIH, Bethesda, MD), anti–FGFR-1 antibody (Sigma-Aldrich Japan), fluorescein isothiocyanate (FITC)–conjugated donkey anti-goat IgG (Santa Cruz Biotechnology), and control mouse IgG1 (Becton Dickinson, San Jose, CA).

Fluorescence-activated cell sorting (FACS) analysis. Staining and flow cytometric analysis of osteoblasts and synovial cells were performed by standard procedures as described previously (14), using a FACScan (Becton Dickinson, Mountain View, CA). Briefly, cells (1×10^5) were incubated with specific mAb and subsequently with FITC-conjugated goat anti-mouse IgG antibody or rabbit anti-goat IgG antibody at saturating concentrations in FACS medium consisting of Hanks' balanced salt solution (Nissui, Tokyo, Japan), 0.5% human serum albumin (Green Cross, Osaka, Japan), and 0.2% NaN_3 (Sigma-Aldrich) for 30 minutes at 4°C. After 3 washes in FACS medium, the cells were analyzed with a FACScan. Amplification of the mAb binding was provided by a 3-decade logarithmic amplifier. Quantification of the cell surface antigens on one cell was performed using beads, QIFIKIT (Dako Japan, Kyoto, Japan).

Osteoclast formation in a coculture system of synovial fibroblasts and peripheral blood mononuclear cells (PBMCs). Subcultured synovial cells (3–5 passages) were composed of synovial fibroblasts, since all of the cells showed fibroblastoid morphology and were completely free of CD3-positive T cells and macrophages, as demonstrated by staining with CD11b or nonspecific esterase according to the method of Fujii et al (15).

PBMCs were derived from samples of peripheral blood using Ficoll-Paque. Briefly, peripheral blood was obtained from healthy donors, diluted 1:1 in PBS, layered onto Ficoll-Paque, and centrifuged at 400*g* for 20 minutes. The interface layer was washed 3 times in PBS and was used as PBMCs. Isolated PBMCs (4×10^5 cells/well) were resuspended in α-minimum essential medium (α-MEM) containing 10% FCS and 50 ng/ml of macrophage colony-stimulating factor (M-CSF) and then seeded in 48-well tissue culture plates (Costar 3548; Corning, Corning, NY). Three days later, adherent cells were used for subsequent cocultures with fibroblasts.

Synovial fibroblasts were added to 48-well plates (1×10^4 cells/well) and cocultured for 9 days in α-MEM containing 10% FCS, 50 ng/ml of M-CSF, and $10^{-7}M$ 1,25-dihydroxyvitamin D_3 ($1,25[OH]_2D_3$). After 9 days of culture, some dishes were stained for tartrate-resistant acid phosphatase (TRAP) as described previously (16); the other dishes were trypsinized and seeded onto dentin slices (4 mm). TRAP-positive multinucleated cells that contained more than 3 nuclei were identified as osteoclasts, and these were counted by light microscopy. On day 11, the dentin slices were placed in NH_4OH (1*N*) for 30 minutes and then cleaned by ultrasonication to remove adherent cells. The dentin slices were then washed with distilled water and stained with hematoxylin and eosin. Bone resorption was evaluated by scanning the area of resorption pits by light microscopy.

Statistical analysis. All data were expressed as the mean ± SD. Differences between groups were examined for statistical significance using the unpaired *t*-test. A *P* value less than 0.05 was considered statistically significant.

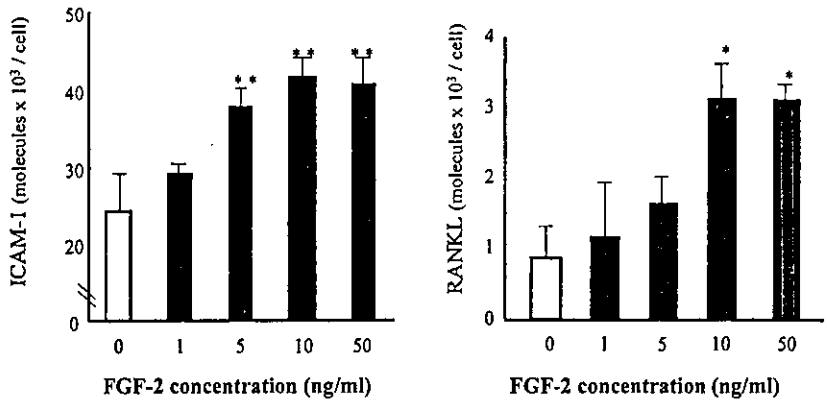

Figure 1. Effects of fibroblast growth factor 2 (FGF-2) on the expression of intercellular adhesion molecule 1 (ICAM-1) and RANKL on synovial fibroblasts from 10 patients with rheumatoid arthritis (RA). RA synovial fibroblasts (RASFs) were incubated with FGF-2 (1–50 ng/ml) for 6 hours, and the levels of ICAM-1 and RANKL expression were analyzed by FACScan. The number of cell surface antigens on a single cell was calculated by QIFIKIT. Values are the mean and SD. * = $P < 0.05$ and ** = $P < 0.01$ versus control (0 ng/ml of FGF-2), by unpaired *t*-test.

RESULTS

We initially assessed the effects of FGF-2 on the expression of ICAM-1 and RANKL on RASFs using a flow cytometer. The indicated amounts of FGF-2 (1–50 ng/ml) were added to the cells, and after 6 hours of incubation, the cells were harvested. The cells were then stained using mAb, analyzed by flow cytometry, and the cell surface antigens on 1 cell were quantified with the use of standard beads. Approximately 25,000 molecules of ICAM-1 and 1,000 molecules of RANKL were spon-

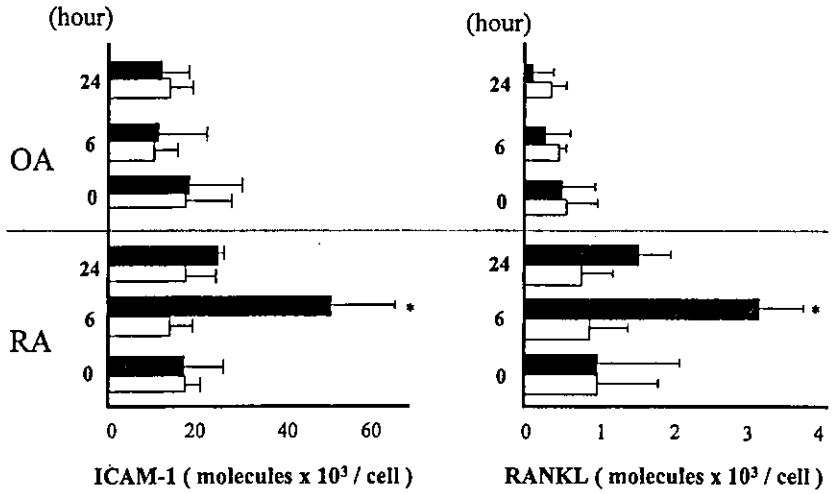

Figure 2. Effects of fibroblast growth factor 2 (FGF-2) on the expression of intercellular adhesion molecule 1 (ICAM-1) and RANKL on synovial fibroblasts from 10 patients with RA and 7 patients with osteoarthritis (OA). OA and RA synovial fibroblasts were incubated with FGF-2 (10 ng/ml) in the presence (open bars) and absence (solid bars) of anti–FGF-2 antibody (10 μg/ml) for the indicated durations, and the levels of ICAM-1 and RANKL expression were analyzed by FACScan. The number of cell surface antigens on a single cell was calculated by QIFIKIT. Values are the mean and SD. * = $P < 0.05$ versus 0 hours of incubation, by unpaired *t*-test.

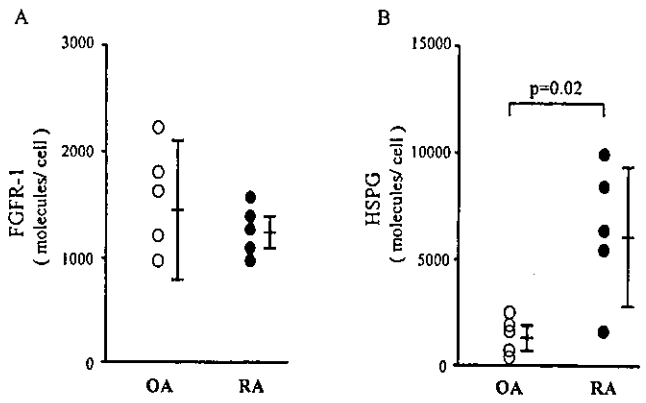

Figure 3. Expression of fibroblast growth factor receptor 1 (FGFR-1) and heparan sulfate proteoglycans (HSPGs) on synovial fibroblasts from 5 patients with rheumatoid arthritis (RA) and 5 patients with osteoarthritis (OA). Staining and flow cytometric analyses of RA and OA synovial fibroblasts were performed with **A**, anti–FGFR-1 antibody or **B**, anti–heparan sulfate monoclonal antibody 10E4, with subsequent staining with fluorescein isothiocyanate–conjugated goat anti-mouse IgG and analysis by FACScan. Values are the mean ± SD. *P* values were determined by unpaired *t*-test.

taneously expressed on RASFs (Figure 1). However, treatment with FGF-2 increased the numbers of both ICAM-1 and RANKL on RASFs in a dose-dependent manner with 6 hours of incubation. In particular, 10 ng/ml of FGF-2 induced 3 times as many RANKL molecules on the cells compared with spontaneous expression. These results indicate that certain concentrations of FGF-2 induce the expression of both RANKL and ICAM-1 on RASFs.

The effects of FGF-2 on the expression of ICAM-1 and RANKL on RASFs from 10 RA patients were compared with the effects on OASFs from 7 OA patients. We found that 10 ng/ml of FGF-2 failed to enhance ICAM-1 and RANKL expression on OASFs after 6 hours or 24 hours of incubation (Figure 2). In contrast, FGF-2 efficiently induced ICAM-1 and RANKL on RASFs, reaching maximum levels within 6 hours. Furthermore, up-regulation of ICAM-1 and RANKL by FGF-2 on RASFs was completely abrogated by the addition of anti–FGF-2 antibody, indicating that FGF-2 plays a pivotal role in the induction of ICAM-1 and RANKL on RASFs.

We next sought to determine why RASFs, but not OASFs, responded to FGF-2 by up-regulating the expression of ICAM-1 and RANKL in an effort to shed light on the receptors for FGF-2. We found that FGFR-1 was similarly expressed on RASFs and OASFs, with ~1,500 sites on 1 cell in these fibroblasts of different origins (Figure 3A). It is well known that HSPGs are coreceptors for FGF-2, promoting both the binding affinity of FGF for FGFR and the subsequent signaling. HSPGs were highly expressed on RASFs, but were only marginally expressed on OASFs (Figure 3B). Furthermore, removal of heparan sulfate from the surface of RASFs by pretreatment with heparitinase or heparinase markedly reduced the up-regulation of RANKL on these cells by FGF-2 (Figure 4). These results imply that the differential responsiveness of RASFs and OASFs to FGF-2 appears to depend on the significantly higher expression of HSPGs on

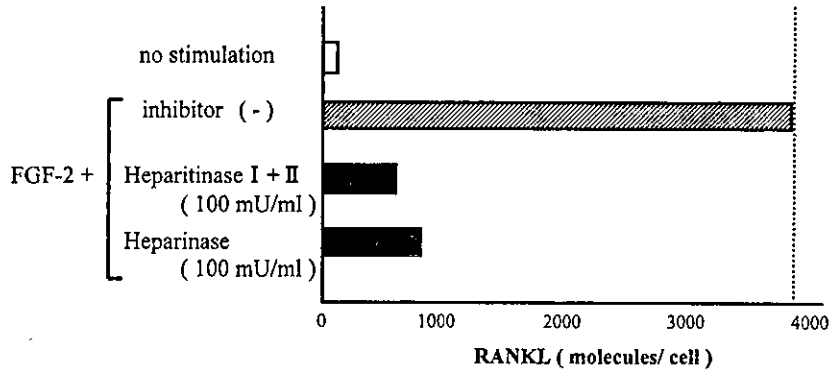

Figure 4. Inhibitory effects of heparitinase and heparinase on fibroblast growth factor 2 (FGF-2)–mediated RANKL expression on synovial fibroblasts from patients with rheumatoid arthritis (RA). RA synovial fibroblasts (RASFs) were treated with a mixture of 100 mU/ml of heparitinase I and II or with heparinase (100 mU/ml) at 37°C for 2 hours. After removal of the added reagents by washing, the RASFs were incubated in the presence or absence of FGF-2 (10 ng/ml) for 6 hours. RANKL expression on RASFs was determined by FACScan. Values are from a representative experiment of cells from 3 RA patients.

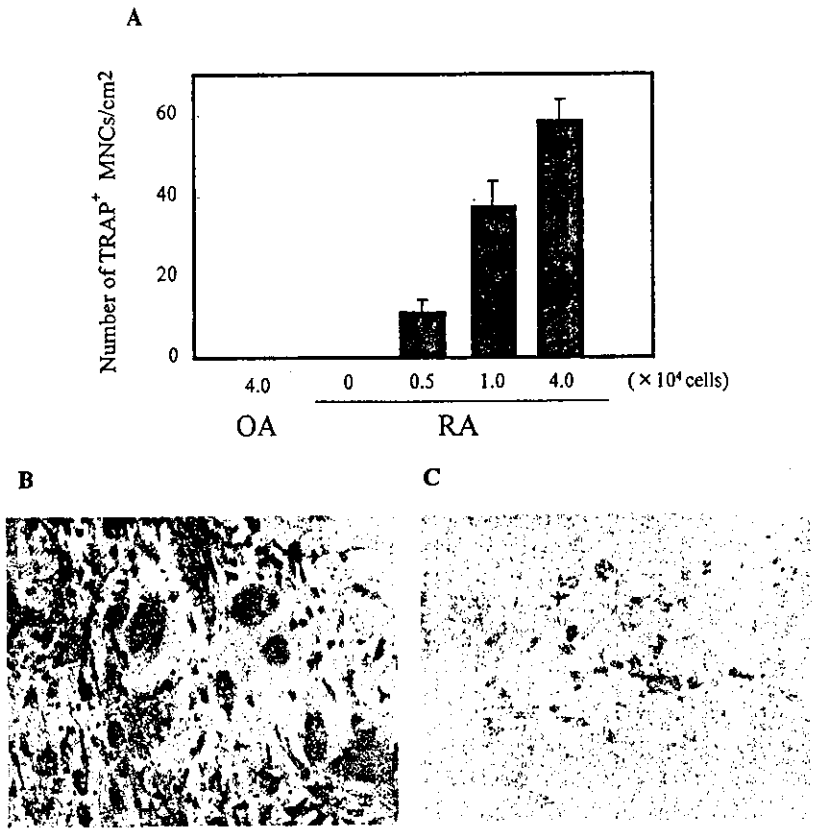

Figure 5. Formation of tartrate-resistant acid phosphatase (TRAP)–positive multinucleated cells (MNCs) from coculture of rheumatoid arthritis synovial fibroblasts (RASFs) and peripheral blood mononuclear cells (PBMCs). Coculture of RASFs and adherent PBMCs was maintained in the presence of 50 ng/ml of macrophage colony-stimulating factor and $10^{-7}M$ 1,25-dihydroxyvitamin D_3 for 9 days, and then the dishes were stained for TRAP. On day 11, dentin slices were placed in NH_4OH (1*N*) for 30 minutes and then cleaned by ultrasonication to remove adherent cells. After washing, the dentin slices were stained with hematoxylin and eosin. TRAP-positive multinucleated cells that contained >3 nuclei were identified as osteoclasts, and these were counted by light microscopy. **A**, Ability of RASFs to support osteoclastogenesis in cocultures with PBMCs. Values are the mean and SD of triplicate measurements. OA = osteoarthritis. **B**, TRAP-positive multinucleated cells in the coculture system. **C**, Resorption pits on dentin slices.

RASFs than that on OASFs and that heparan sulfate present on RASFs might hold FGF-2 as a coreceptor for FGFR-1.

The formation of TRAP-positive multinucleated cells from coculture of RASFs or OASFs (3–5 passages) and PBMCs in α-MEM containing 10% FCS and 50 ng/ml of M-CSF and $10^{-7}M$ $1,25(OH)_2D_3$ was then assessed. After 9 days of culture, there was a marked increase in the number of TRAP-positive multinucleated cells in proportion to the number of RASFs in culture, whereas TRAP-positive multinucleated cells were not induced in cocultures of OASFs and PBMCs (Figure 5A). Furthermore, when the pit-formation assay was performed using the TRAP-positive multinucleated cells induced from the RASF and PBMC coculture, multiple resorption pits were seen on dentin slices, indicating that the TRAP-positive multinucleated cells possess the bone-resorbing function (Figures 5B and C). These results indicate that RASFs, but not OASFs, are involved in osteoclastogenesis and subsequent bone resorption.

The formation of TRAP-positive multinucleated cells by coculture of RASFs and PBMCs was completely inhibited by the addition of anti–FGF-2 antibody, sug-